Clinical Validation of the Automated Characterisation of Cone Size and Centre in Keratoconic Corneas

Bernardo Lopes, MD,PhD[1,2,3], Prema Padmanabhan, MD[4], Haixia Zhang[1,5], PhD, Ahmed Abass, PhD[1], Ashkan Eliasy, MEng, MBA[1], Francisco Bandeira, MD[2], Fanjung Bao, MD[6,7], Jens Bühren, MD[8], Ahmed Elmassry, MD[9], Fernando Faria-Correia, MD, PhD[3,10,11], Karolinne Rocha, MD, PhD[12], Miguel Rechichi, MD, PhD[13], Vito Romano, MD[14,15], Emilio Torres, MD[2,16,17], Riccardo Vinciguerra, MD[1,18], Paolo Vinciguerra, MD[19,20], Ahmed Elsheikh, PhD[1,21,22]

1) School of Engineering, University of Liverpool, Liverpool, UK
2) Department of Ophthalmology and Visual Sciences, Federal University of Sao Paulo, Sao Paulo, Brazil
3) Rio de Janeiro Corneal Tomography and Biomechanics Study Group, Rio de Janeiro, Brazil
4) Department of Cornea and Refractive Surgery, Sankara Nethralaya, Chennai, India.
5) Beijing Advanced Innovation Center for Biomedical Engineering, Beihang University, Beijing, China.
6) School of Ophthalmology and Optometry and Eye Hospital, Wenzhou Medical University, Wenzhou, Zhejiang, China.
7) Key Laboratory of Vision Science, Ministry of Health, Wenzhou, Zhejiang, China.
8) Praxis für Augenheikunde, Frankfurt, Germany.
9) Department of Ophthalmology, Faculty of Medicine, Alexandria University, Egypt.
10) Hospital de Braga, Braga, Portugal.
11) School of Medicine, University of Minho, Braga, Portugal.
12) Storm Eye Institute, Medical University of South Carolina (MUSC), South Carolina, USA
13) Centro Polispecialistico Mediterraneo Sellia Marina, Italy

14) Department of Ophthalmology, Royal Liverpool University Hospital, Liverpool, UK
15) Department of Eye and Vision Science, Institute of Life Course and Medical Sciences, University of Liverpool, Liverpool, UK
16) Laboratory of Cell Biology, Center for Applied Biotechnology and Molecular Medicine, University of Zurich, Switzerland
17) ELZA Institute, Dietikon/Zurich, Switzerland
18) Humanitas San Pio X Hospital, Milan, Italy.
19) Humanitas Clinical and Research Center – IRCCS Rozzano (Mi) – Italy
20) Humanitas University, Department of Biomedical Sciences, Milan, Italy
21) Beijing Advanced Innovation Center for Biomedical Engineering, Beihang University, Beijing, China.
22) NIHR Biomedical Research Centre for Ophthalmology, Moorfields Eye Hospital NHS Foundation Trust and UCL Institute of Ophthalmology, UK.

Dr. Fernando Faria-Correia is a consultant for Alcon

Dr. Ahmed Elmassry is a Consultant of Zeiss Meditec, Gebaur and Novartis.

Dr. Riccardo Vinciguerra reports personal fees from OCULUS, personal fees from OPTIMO MEDICAL, outside the submitted work.

Dr. Paolo Vinciguerra reports personal fees from OCULUS, personal fees from SCHWIND, personal fees from NIDEK, outside the submitted work.

The remaining authors have no financial or proprietary interest in the materials presented herein.

Corresponding author:

Dr.Prema Padmanabhan
Medical Director, Distinguished Senior Consultant, Department of Cornea and Refractive Surgery, Medical Research Foundation, Sankara Nethralaya, 18 College Road, Chennai 600006, Tamil Nadu, India
E-Mail ID:drpp@snmail.org, Tel: 91-44-28271616

Abstract

Purpose: To evaluate an automated method for detecting the cone shape characteristics and to assess the corneal specialists' subjective variability of these measures using different maps.

Methods: Topographic images of the anterior and posterior surface of each eye were presented to 12 clinicians in two different types of map, tangential curvature and relative elevation to the best-fit sphere. They were asked to mark the cone centre and its boundaries in the two maps without knowing that they belong to the same patient. The results between the maps were compared to assess the subjective variability dependent on the map type and the automated method was compared against both estimations to assess its accuracy.

Results: Considering the results of anterior and posterior surfaces, there was low agreement between the cone centre estimations using different types of maps for 10 of the 12 cases ($p<0.05$), while the comparison between the automated method and the two maps estimations did not show differences in 11 of the 12 cases ($p>0.05$). There was high variability, up to 55%, among clinicians' estimations of the cone area. The results of the automated method were within the range of the expert's estimations.

Conclusions: An objective, mathematically derived method of determining morphological dimensions of the cone was consistent with clinicians' evaluations. While there was high variability among the experts' subjective estimates which were highly influenced by the type of map, the objective method provided a reliable evaluation of the keratoconus shape independent of maps or colour-scale.

Key words

Keratoconus

Corneal Topography

Cone Morphology

Introduction

The emergence of a variety of corneal imaging techniques and the use of sophisticated algorithms have enhanced our ability to diagnose early stages of keratoconus.[1] These innovations in technology have largely been driven by the growing popularity of refractive surgery and by the proven efficacy of corneal cross-linking (CXL) in arresting the progression of keratoconus.[2,3] While the emphasis with evolving devices has predominantly been on the accurate detection of keratoconus, even in its subclinical form, relatively less attention has been paid to the use of these techniques in describing the geometrical features of the cone itself.

The cone represents the area of primary pathology in keratoconus.[4] Identifying its location and measuring its magnitude would thus be of seminal importance from a clinician's perspective: in characterising and grading the disease, in tracking its natural course and response to treatment, in the success of specialised contact lens fitting, in facilitating the appropriate placement of Intrastromal Corneal Ring Segments (ICRS) and in the design of customised CXL procedures in the future.

There have been few attempts to map cone location, the definitions, assumptions and methodology of each being different and often instrument-dependent.[5-8] With no consensus on a standardised approach to assess the area occupied by the cone, clinicians are forced to exercise their judgement and make subjective assessments based on colour-coded tomography maps.

In response to this need, Eliasy et al proposed a robust, objective and accurate method to delineate the location and 3-dimensional magnitude of the cone in eyes with clinically diagnosed keratoconus.[9] The present study aims to evaluate this automated method against the subjective estimates of 12 cornea specialists and to assess the subjective variability of those assessments among the examiners.

Methods

This study was conducted according to the tenets of the Declaration of Helsinki. In the study, an anonymised database of corneal tomography examinations obtained with Pentacam HR (Oculus, Wetzlar, Germany) from patients diagnosed with keratoconus was reviewed. As only fully anonymised secondary data was used, according to the University of Liverpool's Policy on Research Ethics, ethical approval was ruled unnecessary. The maps were grouped according to the Pentacam's Topographic Keratoconus Classification (TKC) in mild – grades: "abnormal", "possible", "–" and 1; moderate – grades: 1 to 2, 2, and 2 to 3; and advanced:– grades 3, 3 to 4, and 4.[10] One eye of two patients from each group – a total of 6 cases – were randomly selected. Tangential curvature and relative elevation to the best-fit sphere maps were generated for both corneal surfaces using Pentacam software version 1.20b94. The absolute Smolek–Klyce 1.5 D scale was used in the tangential curvature maps and the relative Belin intuitive 2.5µm scale was used in the relative elevation maps. The coordinates of the points of maximum curvature on the tangential map and of the maximum elevation on the relative elevation map were recorded.

Four figures, each containing the maps for both anterior and posterior surfaces were prepared for the six selected patients in a shuffled order as observed in Figure 1. The resulting 24 images in the four figures were sent to 12 cornea specialists from across the globe with the instruction that they belonged to 24 different patients for masked subjective location of the cone centre and estimation of its boundaries. The marked images were processed with MATLAB Image Processing Toolbox (11.1, The MathWorks, Inc., Natick, Massachusetts, United States) and the coordinates of the cone centre and estimated boundaries, along with the area of the disease, were stored in a binary file.

In addition to the clinicians' markings, the cone centre, boundaries and disease area, in each of the corneal surfaces of the six cases were also estimated by custom-built MATLAB (2020a, The MathWorks, Inc., Natick, Massachusetts, United States) codes created by the

Biomechanical Engineering Group (BioEG) at the University of Liverpool, as described previously.[9] In brief, the process works as follows: the central 8 mm diameter area of the raw elevation data was fitted to a sphere using the least-squares method. The centre coordinates of the optimal fit sphere were used as a reference to calculate the radial distance of each point on the corneal surface. The radial distances were then subtracted from the radius of the optimal sphere and the position of the point with the largest positive difference defined the cone centre and height. The next steps to estimate the area of the pathology were conducted as follows: the radial height data relative to the optimal sphere were determined along 360 equally spaced lines meeting at the cone centre and extending outwards using triangle-based cubic interpolation. The first derivative was calculated to determine the tangent to the surface along the height data. The second derivative was then calculated to identify the rate of change in the tangent gradient. Sudden variations in the rate of gradient change indicated the transition zone between the cone area and healthy surrounding tissue. Finally, an iterative process was conducted. The cone area was removed from the raw elevation data prior to re-identifying the optimal sphere and the aforementioned steps were repeated. The process was concluded when two subsequent analyses produced results (cone height and centre location) with differences smaller than 1.0 µm.

Due to the non-normality of the data distribution (Shapiro-Wilk test, $p<0.05$), the variables were described by median, interquartile range (IQR), minimum and maximum. The comparison of the clinicians' estimates of the cone centre and area using the different maps was performed with Wilcoxon's signed-rank test. The distances among the cone centre positions between the subjective estimates using tangential and relative elevation maps; and the automated objective method were assessed with the Friedman's test one-way repeated-measures analysis of variance. The variation among the experts' estimations of the cone area was assessed with the non-parametric coefficient of variation (median absolute deviation divided by the median). The sample size was calculated based on the estimations of 4 corneal specialists obtained in a trial case. To detect a difference between the maps of 0.3 ± 0.2 mm

in cone centre and 2 ± 2 mm^2 in cone area, using a 2-sided level of significance (α) = 5% and power (1-β) = 80%, it was required the estimations of 10 corneal specialists. A number 20% higher was used in this study to account for the relatively lower power of non-parametric tests. Statistical analyses were accomplished using R Core Team (2016, R: A language and environment for statistical computing. R Foundation for Statistical Computing, Vienna, Austria).

Results

The demographic characteristics of the six cases included are summarised in table 1. Regarding the cone centre position, there was a good match between the clinicians' estimations and the tomographer's points of maximum curvature of the tangential map or maximum elevation on the relative elevation to the best-fit sphere map, in both corneal surfaces. However, the values were statistically significantly different between the maps ($p<0.05$) on the posterior surface of all cases and on the anterior surface of all of them, apart from cases 3 and 6. The agreement among the clinicians' estimations and the automated estimation was high, the distances between these three centre estimates were not statistically significant, apart from the anterior surface of case 1. These results are summarised in table 2 and figure 2.

Regarding the area of the disease, on the anterior surface the clinicians' estimations were larger on the tangential map than on the relative elevation map for all cases ($p<0.001$). The same pattern was observed on the posterior surface for 4 of the 6 cases. There was high variation among the clinicians' estimations. For the anterior surface, the non-parametric coefficient of variation (npCV) was 20.5% (19.7, 13.0 –55.0%, IQR (minimum – maximum)) on the tangential map and 30.3% (10.2, 17.0 –40.7%) on the relative elevation map. For the posterior surface, it was 24.5% (8.2, 12.0 –35.0%) on the tangential map and 22.2% (3.6, 15.2 –36.3%) on the relative elevation map. The automated detection presented values in between

188 the clinicians' estimates for all cases on both surfaces of both maps. Table 3 summarises
189 these results.

190 **Discussion**

191 The present study evaluated the ability of a new automated method to detect the cone centre
192 and the boundaries of the cone and compared them with the subjective estimates provided by
193 12 experienced corneal specialists. A bias towards the point of maximum curvature in the
194 tangential maps or to the highest point on the relative elevation map was observed in the
195 clinicians' estimations of the cone centre even if, for the same case, they were significantly
196 distant from each other. A similar bias was also observed in the estimation of the boundaries
197 and interestingly high variations, up to 55%, were present for the same case among the
198 examiners. While there was high subjective variability, the results produced by the automated
199 method were, by and large, in agreement with the clinicians' estimates.

200 Before the advent of corneal videokeratography, keratoconus was broadly described based
201 on the shape and location of the cone. Nipple cones had central conical protrusions and oval
202 cones had inferior sagging projections. However, these gross descriptions were possible only
203 when the disease was clinically obvious or detectable by keratoscopy.[11] The advent of
204 computerized videokeratoscopes, which captured information from thousands of points on the
205 anterior corneal surface to produce detailed colour-coded maps allowed identification of
206 subtler changes in curvature. Diverse patterns of normal and abnormal corneas were now
207 recognizable.[12] The development of topographic indices and neural networks made the
208 corneal topographer a diagnostic instrument to detect pathology[13] and led to the incorporation
209 of automated keratoconus detection systems into commercial videokeratographic devices.[14]
210 The standardization of colour scales of topographic maps underwent multiple revisions to
211 facilitate a distinction between normal and abnormal patterns, which clinicians could adopt in
212 routine practice.[15] The recognition of the limitations of curvature based maps and the
213 importance of measuring changes in the posterior corneal surface and corneal thickness led

to the introduction of elevation based devices.[16] The concept of corneal tomography, as opposed to topography was thus introduced and its ability to represent the corneal shape in its three-dimensional entirety was amply demonstrated. The more recently developed devices using high-frequency ultrasound and the anterior segment optical coherence tomography (AS-OCT) are able to enhance the corneal shape characterisation by evaluating the behaviour of its individual layers.[17] Kanellopoulos and Asimellis have demonstrated with AS-OCT an in-vivo ability of the corneal epithelium to smooth the corneal surface by becoming thinner over the cone apex and thicker around it, which acts as a confounding factor for the keratoconic cornea shape analysis.[18] The authors also studied this imaging technique's ability to differentiate healthy and keratoconus corneas even in early stages of the disease.[19,20]

The growing interest in improving methods to detect early keratoconus is sustained by two important factors: the evidence for a successful therapeutic option for keratoconus and the importance of being able to identify eyes that are at risk of developing ectasia following laser refractive procedures.[21,22] Several new algorithms have been introduced in recent years, including some that integrate tomographic features with corneal biomechanical parameters that are able to discriminate normal from keratoconic eyes with a high degree of sensitivity and specificity.[23,24] Relatively less attention has been paid to accurately demarcate the boundaries of the cone or to characterize its three-dimensional features. The cone represents the area of primary pathology in keratoconus. Hence, studying its morphology and the dynamics of changes that occur either in its natural time course or in response to treatment would significantly enhance our understanding of the disease and improve our approach to its management.

Although keratoconus is recognized as a progressive disease, there is no consensus yet on an ideal system of classification.[25] Belin and Duncan recently proposed a new classification system incorporating data from both surfaces of the cornea in a 3mm zone centred around the thinnest point – a zone chosen to reflect the major ectatic region of the cornea.[26] This new

system not only independently grades the anterior and posterior radii of curvature, the thinnest corneal pachymetry in this zone, has a modifier component for scarring and, for the first time, includes the vital functional component of vision. Although more comprehensive than any other grading system yet proposed, it does not capture other descriptors of the cone itself, like the area occupied, its location and the degree of decentration of its apex, all of which could have useful clinical implications.

The maximum keratometry (Kmax) has been the commonly used parameter to detect and document progression in ectasia. However, Kmax often fails to reflect the true degree of ectasia, ignores the contribution of the posterior cornea to progression and due to its high variability in KC cases, the traditional threshold used to detect progression commonly lack accuracy.[27,28] The Global Consensus on Keratoconus and Ectasia defined progression by a consistent change in any 2 of 3 parameters (steepening of the anterior corneal surface, steepening of the posterior corneal surface and changes in pachymetric rate of change),[25] without the need to demarcate the cone although all 3 parameters were likely descriptors of changes happening within the cone itself. Changes in the area of the cone, if measurable, could be an additional feature of progression, one that has been hitherto ignored. It would also be of interest to study distinct patterns in progression, if any, for example in response to eye rubbing.

Knowledge of the cone morphology would further be invaluable in planning the appropriate contact lens fitting.[29] The type of lens, its size and the fitting philosophy all depend on cone characteristics.[30]

The choice of type, shape, arc length and location of placement of ICRS in the treatment of keratoconus and the decision to combine it with adjunctive procedures would be influenced by individual cone characteristics.[31]

Corneal cross-linking (CXL) as a treatment to prevent progression of keratoconus has been proven and accepted globally. The location of the cone may affect the outcome of the

procedure and may have an effect on the quality of vision.[32] Therefore, differentiating keratoconus based on cone location may reveal differences in the course of disease as well as in their response to treatment. Efforts to refine the procedure and minimize its drawbacks led to the concept of customized CXL.[33] Recently Seiler et al reported a successful outcome with concentric zones of CXL centred around the maximum posterior float.[34] An accurate delineation of the cone would allow the creation of customized protocols which would retain the intended benefits of CXL without unnecessary exposure of healthy tissue to irradiance.

Currently, there is no consensus on how cone morphology is best defined or measured. Cone location is typically denoted by the sector of decentration of the cone apex. The cone apex, in turn, has been defined as the point on a topographic map, showing the highest dioptric power either using the axial/sagittal display (global representations of curvature) or the tangential display (which represent local curvature by spatial location)[35] although Schwiegerling clearly emphasized that techniques using dioptric power to locate the cone apex could be misleading.[5] The recognition that the steepest area may not be the area of greatest protrusion made elevation-based maps more useful in locating the cone apex, now defined as the point with highest positive deviation in microns, from the Best fit sphere.[36] Some authors consider the thinnest point on the cornea to represent the centre of the cone. Interestingly, Tu et al have shown that the keratometric apex, the elevation apex and the pachymetry apex most often do not coincide in eyes with keratoconus.[37] Mahmoud AM et al introduced CLMI as an index to determine the location and curvature magnitude of the cone as described by an algorithm that was applied to axial and tangential curvature maps.[38] The CLMI_X was subsequently proposed as an extension of the CLMI algorithm to include the combination of tomographic information from the anterior and posterior surfaces of the cornea as well as corneal thickness to make it a more robust index to detect ectasia.[39] The CLMI and CLMI_X, not being intended to be descriptors of cone morphology, have proved themselves useful in being a sensitive diagnostic tool.

The assessment of cone pattern and size, on the other hand, is largely based on subjective pattern recognition, choosing the 2 warmest colours displayed on colour coded maps. Rabinowitz et al described 10 topographic patterns which formed a template often used by clinicians to label patients with keratoconus.[40]

The paucity of precise, objective, technique to delineate the cone and the need for a robust technology to do so forms the basis of the method proposed by Eliasy et al and used in this study.[9] The method is universal and can be applied to corneal topographic images from different sources such as Placido's topography, Scheimpflug and OCT tomographies, including the segmental OCT stromal maps that are able to mitigate the influence of varying epithelial thickness.

The cone morphology estimated by the 12 experienced topography readers on the same patients using two different maps were significantly different ($p<0.001$) for all cases on the anterior surface and three cases on the posterior surface. The inter-observer variation was up to 40.8% on the relative elevation maps and up to 55% on the tangential maps. Ramos et al[37] reported high subjective variability among 11 corneal topography specialists who were asked to classify the topographic exam of 25 eyes with absolute colour-scale system and again with normative scales without knowing that they were being presented the same cases. In 44% of cases using normative scales a variation in classification between 0 to 4 was found across the examiners. Using different scales the same examiner had given different classifications in 56% of cases. In the present study, the results obtained with the automated method were within the interquartile range (IQR, corresponds to the central 50% of values of the sample) for all cases on the anterior surface. On the posterior surface, even though the estimates were slightly lower than the boundary of the IQR they were within the limits of the experts' estimations. While the subjective classification is somehow limited by the colour-scale, the automated method, with its iterative process, in addition to not relying on scales, allows for a better peripheral fitting and a more precise identification of the protruded area.

The small sample size was a limitation of the study, which, however, did not affect the primary goal of the study which was to evaluate how the automated process would perform in relation to clinicians' classification. It could be argued that the simulated conditions in this study for experts to make their evaluation solely on the basis of corneal images rather than on clinical details may have been unrealistic. However, the masked analysis used in this study was deliberately chosen to allow a direct comparison of how the experts interpreted the images without been influenced by their clinical judgement.

Future studies will explore the effect of cone geometry on refractive errors, higher-order aberrations and image quality. The dynamics of cone geometry with disease progression, as well as the response of cone characteristics to corneal procedures such as corneal cross-linking and ICRS implantation along with the implementation of machine learning techniques to improve the mathematical method are also future projects.

In summary, an automated method to describe the cone in its 3D geometry fulfilled the need for an objective assessment that is free of color-scale bias while clinical estimations showed significant variability.

334 **Legends**

335 Table 1: Patient's demographic characteristics.

336 Table 2: Cone centre estimations in mm relative to corneal apex by experts using tangential
337 curvature and relative elevation maps along with results of the automated method.

338 Table 3 Cone area estimations in mm2 by experts using tangential curvature and relative
339 elevation maps along with the automated method.

340

Figure 1 Corneal images of the 6 patients included

Caption: A: Tangential curvature map of the anterior surface. B: Tangential curvature map of the posterior surface. C: Relative elevation to best-fit sphere map of the anterior surface. D: Relative elevation to best-fit sphere map of the posterior surface.

Figure 2 Cone centre estimations relative to corneal apex by experts using tangential curvature and relative elevation maps along with results of the automated method.

Caption: A to F: Anterior surface of cases 1 to 6. G to L: Posterior surface of cases 1 to 6. Blue circle: centre of cone estimated by the automated method. Red circle: experts' average estimation of cone centre on relative elevation maps. Green circle: experts' average estimation of cone centre on tangential curvature maps. (X and Y axes units: mm)

Figure 3 Cone geometry estimations by experts using tangential curvature and relative elevation maps along with results of the automated method.

Caption: A to F: anterior surface of cases 1 to 6. G to L: posterior surface of cases 1 to 6. Blue line: cone boundaries estimated by the automated method. Red lines: experts' cone boundaries estimations on relative elevation maps. Green lines: experts' cone boundaries estimations on tangential curvature maps. (X and Y axes units: mm)

References

1. Mas Tur V, MacGregor C, Jayaswal R, O'Brart D, Maycock N. A review of keratoconus: Diagnosis, pathophysiology, and genetics. *Surv Ophthalmol.* 2017;62(6):770-783.
2. Lin SR, Ladas JG, Bahadur GG, Al-Hashimi S, Pineda R. A Review of Machine Learning Techniques for Keratoconus Detection and Refractive Surgery Screening. *Semin Ophthalmol.* 2019;34(4):317-326.
3. Li W, Wang B. Efficacy and safety of transepithelial corneal collagen crosslinking surgery versus standard corneal collagen crosslinking surgery for keratoconus: a meta-analysis of randomized controlled trials. *BMC Ophthalmol.* 2017;17(1):262.
4. Prakash G, Srivastava D, Choudhuri S, Thirumalai SM, Bacero R. Differences in central and non-central keratoconus, and their effect on the objective screening thresholds for keratoconus. *Acta Ophthalmol.* 2016;94(2):e118-129.
5. Schwiegerling J. Cone dimensions in keratoconus using Zernike polynomials. *Optom Vis Sci.* 1997;74(11):963-969.
6. Demirbas NH, Pflugfelder SC. Topographic pattern and apex location of keratoconus on elevation topography maps. *Cornea.* 1998;17(5):476-484.
7. Colin J, Sale Y, Malet F, Cochener B. Inferior steepening is associated with thinning of the inferotemporal cornea. *J Refract Surg.* 1996;12(6):697-699.
8. Auffarth GU, Wang L, Volcker HE. Keratoconus evaluation using the Orbscan Topography System. *J Cataract Refract Surg.* 2000;26(2):222-228.
9. Eliasy A, Abass A, Lopes BT, Vinciguerra R, Zhang H, Vinciguerra P, Ambrósio Jr R, Roberts CJ, Elsheikh A. 2020 Characterization of cone size and centre in keratoconic corneas. *J. R. Soc.* Interface 17: 20200271

10. Goebels S, Eppig T, Wagenpfeil S, Cayless A, Seitz B, Langenbucher A. Staging of keratoconus indices regarding tomography, topography, and biomechanical measurements. *Am J Ophthalmol.* 2015;159(4):733-738.

11. Rabinowitz YS, McDonnell PJ. Computer-assisted corneal topography in keratoconus. *Refract Corneal Surg.* 1989;5(6):400-408.

12. Bogan SJ, Waring GO, 3rd, Ibrahim O, Drews C, Curtis L. Classification of normal corneal topography based on computer-assisted videokeratography. *Arch Ophthalmol.* 1990;108(7):945-949.

13. Maeda N, Klyce SD, Smolek MK. Neural network classification of corneal topography. Preliminary demonstration. *Invest Ophthalmol Vis Sci.* 1995;36(7):1327-1335.

14. Maeda N, Klyce SD, Smolek MK. Comparison of methods for detecting keratoconus using videokeratography. *Arch Ophthalmol.* 1995;113(7):870-874.

15. Smolek MK, Klyce SD, Hovis JK. The Universal Standard Scale: proposed improvements to the American National Standards Institute (ANSI) scale for corneal topography. *Ophthalmology.* 2002;109(2):361-369.

16. Ambrosio R, Jr., Alonso RS, Luz A, Coca Velarde LG. Corneal-thickness spatial profile and corneal-volume distribution: tomographic indices to detect keratoconus. *J Cataract Refract Surg.* 2006;32(11):1851-1859.

17. Urs R, Lloyd HO, Reinstein DZ, Silverman RH. Comparison of very-high-frequency ultrasound and spectral-domain optical coherence tomography corneal and epithelial thickness maps. *J Cataract Refract Surg.* 2016;42(1):95-101.

18. Kanellopoulos AJ, Asimellis G. Anterior segment optical coherence tomography: assisted topographic corneal epithelial thickness distribution imaging of a keratoconus patient. *Case Rep Ophthalmol.* 2013;4(1):74-78.

19. Kanellopoulos AJ, Asimellis G. OCT-derived comparison of corneal thickness distribution and asymmetry differences between normal and keratoconic eyes. *Cornea.* 2014;33(12):1274-1281.

20. Kanellopoulos AJ, Asimellis G. OCT corneal epithelial topographic asymmetry as a sensitive diagnostic tool for early and advancing keratoconus. *Clin Ophthalmol.* 2014;8:2277-2287.

21. Wollensak G, Spoerl E, Seiler T. Riboflavin/ultraviolet-a-induced collagen crosslinking for the treatment of keratoconus. *Am J Ophthalmol.* 2003;135(5):620-627.

22. Randleman JB, Woodward M, Lynn MJ, Stulting RD. Risk assessment for ectasia after corneal refractive surgery. *Ophthalmology.* 2008;115(1):37-50.

23. Luz A, Lopes B, Hallahan KM, Valbon B, Ramos I, Faria-Correia F, Schor P, Dupps WJ, Ambrósio R. Enhanced Combined Tomography and Biomechanics Data for Distinguishing Forme Fruste Keratoconus. *J Refract Surg.* 2016;32(7):479-494.

24. Ambrosio R, Jr., Lopes BT, Faria-Correia F, Salomão MQ, Bühren J, Roberts CJ, Elsheikh A, Vinciguerra R, Vinciguerra P. Integration of Scheimpflug-Based Corneal Tomography and Biomechanical Assessments for Enhancing Ectasia Detection. *J Refract Surg.* 2017;33(7):434-443.

25. Gomes JA, Tan D, Rapuano CJ, Belin MW, Ambrósio Jr R, Guell JL, Malecaze F, Nishida K, Sangwan VS. Global consensus on keratoconus and ectatic diseases. *Cornea.* 2015;34(4):359-369.

26. Belin MW, Duncan JK. Keratoconus: The ABCD Grading System. *Klin Monbl Augenheilkd.* 2016;233(6):701-707.

27. Duncan JK, Belin MW, Borgstrom M. Assessing progression of keratoconus: novel tomographic determinants. *Eye Vis (Lond).* 2016;3:6.

28. Guilbert E, Saad A, Elluard M, Grise-Dulac A, Rouger H, Gatinel D. Repeatability of Keratometry Measurements Obtained With Three Topographers in Keratoconic and Normal Corneas. *J Refract Surg.* 2016;32(3):187-192.

29. Downie LE, Lindsay RG. Contact lens management of keratoconus. *Clin Exp Optom.* 2015;98(4):299-311.

30. Sorbara L, Dalton K. The use of video-keratoscopy in predicting contact lens parameters for keratoconic fitting. *Cont Lens Anterior Eye.* 2010;33(3):112-118.

31. Park SE, Tseng M, Lee JK. Effectiveness of intracorneal ring segments for keratoconus. *Curr Opin Ophthalmol.* 2019;30(4):220-228.

32. Tan B, Baker K, Chen YL, Lewis JW, Shi L, Swartz T, Wang M. How keratoconus influences optical performance of the eye. *J Vis.* 2008;8(2):13 11-10.

33. Sinha Roy A, Dupps WJ, Jr. Patient-specific computational modeling of keratoconus progression and differential responses to collagen cross-linking. *Invest Ophthalmol Vis Sci.* 2011;52(12):9174-9187.

34. Seiler TG, Fischinger I, Koller T, Zapp D, Frueh BE, Seiler T. Customized Corneal Cross-linking: One-Year Results. *Am J Ophthalmol.* 2016;166:14-21.

35. Cavas-Martinez F, De la Cruz Sanchez E, Nieto Martinez J, Fernandez Canavate FJ, Fernandez-Pacheco DG. Corneal topography in keratoconus: state of the art. *Eye Vis (Lond).* 2016;3:5.

36. Belin MW, Khachikian SS. An introduction to understanding elevation-based topography: how elevation data are displayed - a review. *Clin Exp Ophthalmol.* 2009;37(1):14-29.

37. Tu KL, Tourkmani AK, Srinivas S. Interrelationships Between 3 Keratoconic Cone Parameters. *Cornea.* 2017;36(9):1051-1053.

38. Mahmoud AM, Roberts CJ, Lembach RG, Twa MD, Herderick EE, McMahon TT, CLEK Study Group. CLMI: the cone location and magnitude index. *Cornea.* 2008;27(4):480-487.

39. Mahmoud AM, Nunez MX, Blanco C, Koch DD, Wang L, Weikert MP, Frueh BE, Tappeiner C, Twa MD, Roberts CJ. Expanding the cone location and magnitude index to include corneal thickness and posterior surface information for the detection of keratoconus. *Am J Ophthalmol.* 2013;156(6):1102-1111.

40. Rabinowitz YS, Yang H, Brickman Y, Akkina J, Riley C, Rotter JI, Elashoff J. Videokeratography database of normal human corneas. *Br J Ophthalmol.* 1996;80(7):610-616.

41. Ramos IC, Correa R, Guerra FP, Trattler W, Belin MW, Klyce SD, Fontes BM, Schor P, Smolek MK, Dawson DG, Chalita MR. Variability of subjective classifications of corneal topography maps from LASIK candidates. *J Refract Surg.* 2013;29(11):770-775.

Table 1: Patient's demographic characteristics.

	Case 1	Case 2	Case 3	Case 4	Case 5	Case 6
Age	39	42	49	31	28	62
Gender	Female	Female	Female	Male	Male	Male
Eye	Left	Right	Right	Right	Left	Left
TKC	# 1	# 1	# 2-3	# 2-3	# 3-4	# 3
K Max (D)	46.8	50.7	58.1	54.3	67.9	57.5
Pachy Apex (µm)	528	444	491	399	424	439
Pachy Min (µm)	507	429	473	386	397	411

TKC: Pentacam's topographic keratoconus classification; K Max: maximum curvature of the anterior surface. Pachy apex: corneal thickness at the apex; Pachy min: minimum corneal thickness.

Table 2

Table 2: Cone centre estimations in mm relative to corneal apex by experts using tangential curvature and relative elevation maps along with results of the automated method

		Tangential Map				Relative Elevation Map				Experts' estimates between maps	Automated Detection		Distance between estimations in each map and automated detection
		Pentacam		Experts' Estimates		Pentacam		Experts' Estimates		p-value			p-value
		X	Y	X (median(IQR))	Y (median(IQR))	X	Y	X (median(IQR))	Y (median(IQR))		X	Y	
Anterior Surface	Case 1	0.1	-1.4	0.1 (0.05)	-1.4 (0.04)	0.8	-1.4	0.8 (0.03)	-1.4 (0.04)	0.003	0.6	-1.3	0.019
	Case 2	-0.1	-0.6	-0.1 (0.01)	-0.6 (0.09)	-0.3	-0.5	-0.3 (0.16)	-0.5 (0.04)	0.024	-0.3	-0.5	0.243
	Case 3	0.1	-0.9	0.1 (0.04)	-0.9 (0.04)	-0.1	-1.0	-0.1 (0.08)	-1.0 (0.05)	0.099	-0.1	-1.0	0.169
	Case 4	-0.4	-0.7	-0.4 (0.01)	-0.7 (0.12)	-0.8	-1.1	-0.8 (0.03)	-1.1 (0.08)	0.003	-0.8	-1.1	0.088
	Case 5	-0.5	-0.5	-0.5 (0.09)	-0.5 (0.13)	0.0	-0.9	0.0 (0.01)	-0.9 (0.05)	0.002	0.1	-0.8	0.243
	Case 6	-0.1	-2.8	-0.1 (0.01)	-2.8 (0.10)	-0.1	-2.6	-0.1 (0.02)	-2.6 (0.04)	0.184	0.0	-2.0	0.169
Posterior Surface	Case 1	0.1	-1.2	0.1 (0.01)	-1.2 (0.02)	0.3	-1.3	0.3 (0.04)	-1.3 (0.04)	0.008	0.5	-1.3	0.112
	Case 2	-0.2	-0.5	-0.2 (0.28)	-0.5 (0.09)	-0.6	-0.7	-0.6 (0.04)	-0.7 (0.04)	0.002	-0.5	-0.6	0.284
	Case 3	-0.2	-0.6	-0.2 (0.08)	-0.6 (0.06)	-0.7	-0.8	-0.7 (0.04)	-0.8 (0.04)	0.002	-0.6	-0.7	0.169
	Case 4	-0.4	-0.8	-0.4 (0.04)	-0.8 (0.08)	-0.7	-1.1	-0.7 (0.06)	-1.1 (0.06)	0.003	-0.7	-1.1	0.052
	Case 5	0.1	-1.0	0.1 (0.04)	-1.0 (0.04)	0.2	-1.1	0.2 (0.08)	-1.1 (0.06)	0.003	0.2	-1.0	0.169
	Case 6	-0.3	-2.1	-0.3 (0.04)	-2.1 (0.04)	-0.5	-2.0	-0.5 (0.08)	-2.0 (0.05)	0.004	-0.5	-1.9	0.169

X: x-axis coordinates of cone centre in mm; Y: y-axis coordinates of cone centre in mm; IQR: interquartile range.

Table 3

Cone area estimations in mm^2 by experts using tangential curvature and relative elevation maps along with the automated method

	Tangential Map					Relative Elevation Map						
	Median	IQR	Min	Max	npCV	Median	IQR	Min	Max	npCV	p-value	Automated Detection
Anterior Surface	7.8	4.6	3.8	17.8	55.0%	5.6	2.0	2.0	8.8	32.5%	<0.001	6.6
	17.2	1.8	7	23.6	13.0%	6.4	2.4	4.5	10.7	40.8%	<0.001	10.1
	11.3	2.7	8.5	19.8	24.4%	7.9	3.0	5.3	11.4	39.3%	<0.001	6.8
	14.4	9.2	6.5	25.3	40.1%	9.5	2.6	7.5	13.1	28.2%	<0.001	8.6
	14.4	2.6	3.9	24.5	15.6%	8.5	2.5	6.7	12.2	27.2%	<0.001	9.6
	19.6	3.6	2.8	27.3	17.4%	11.7	2.0	8.6	18.9	17.0%	<0.001	11.9
Posterior Surface	7.7	3.0	3.6	10.9	35.0%	8.3	1.6	5.7	11.4	20.5%	0.791	5.0
	9.7	4.6	7.6	18.8	28.5%	5.7	1.9	4.5	8.5	36.3%	<0.001	7.0
	11.0	2.9	8.6	25.4	23.0%	9.4	1.5	5.6	12.0	15.2%	0.012	6.5
	10.3	3.1	8.0	19.8	13.3%	11.1	2.8	9.7	16.0	23.1%	0.733	8.3
	14.3	2.7	11.9	20.6	18.8%	11.3	3.0	4.6	17.0	24.8%	<0.001	8.1
	16.0	3.5	9.1	21.7	25.7%	14.1	2.8	8.4	22.7	21.3%	0.092	10.0

IQR: Interquartile range; npCV: non-parametric coefficient of variation

Figure 1A

Click here to access/download;Figure;Figure1A.tiff

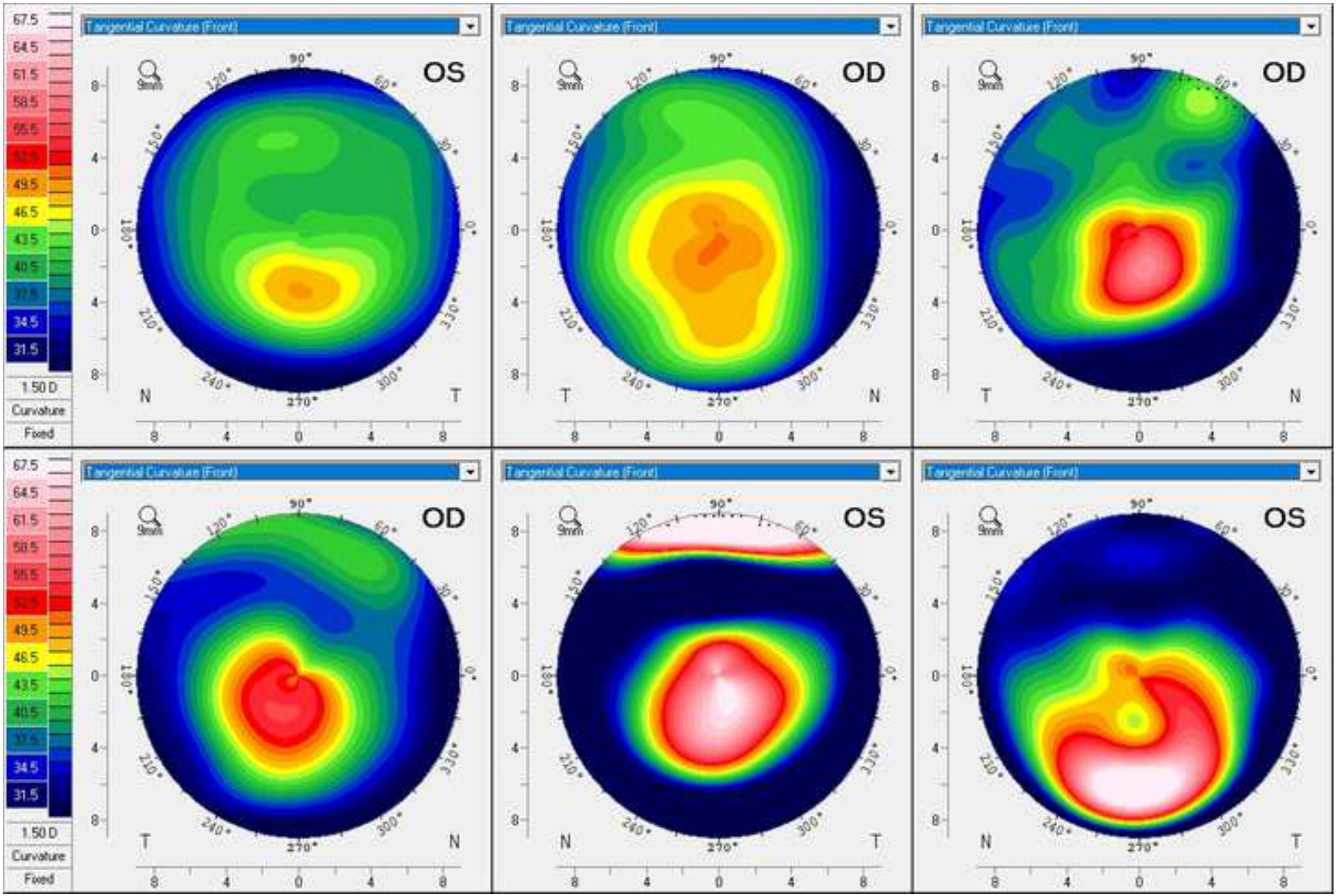

Figure 1B

Click here to access/download;Figure;Figure1B.tiff

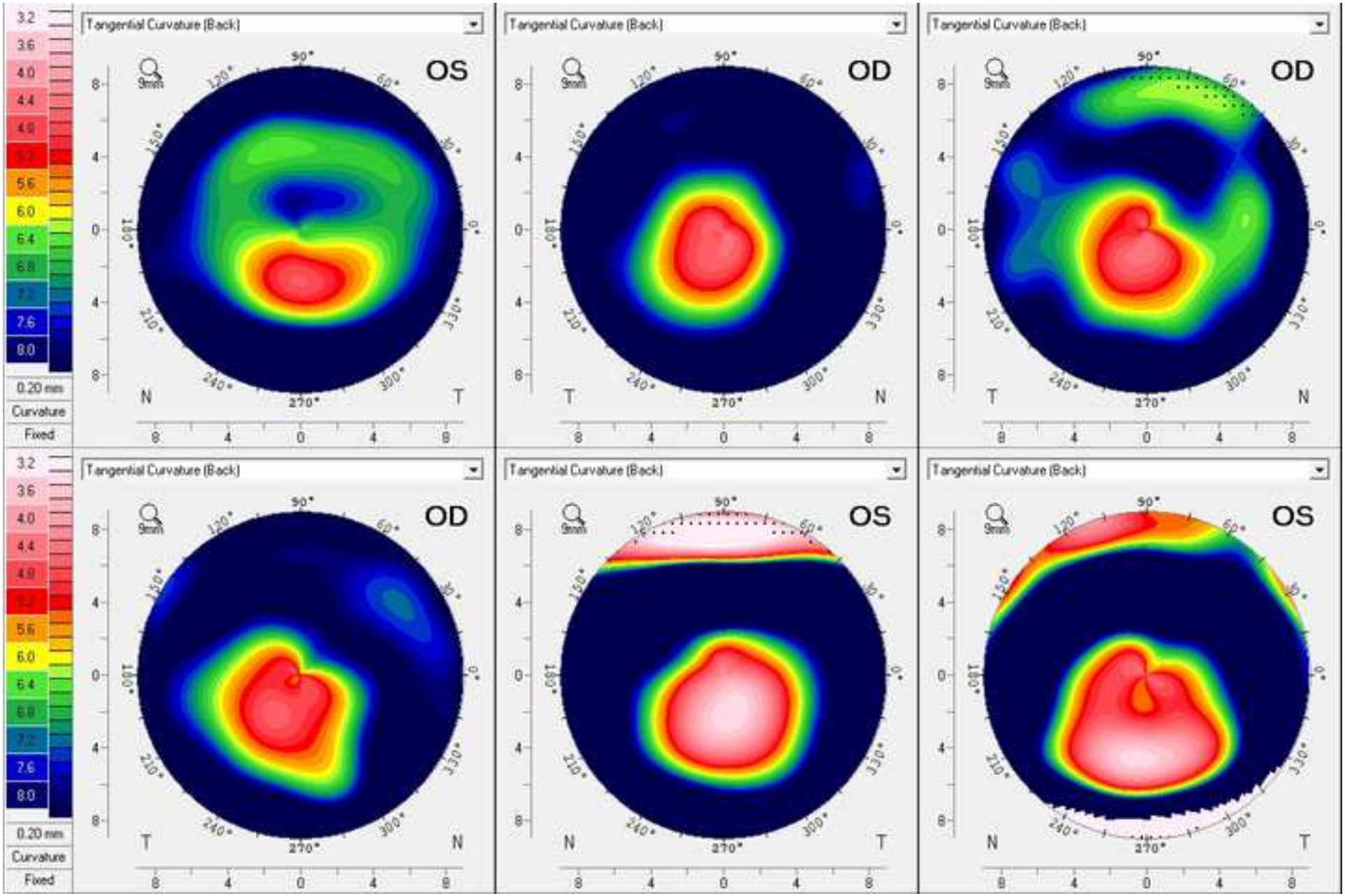

Figure 1C

Click here to access/download;Figure;Figure1C.tiff

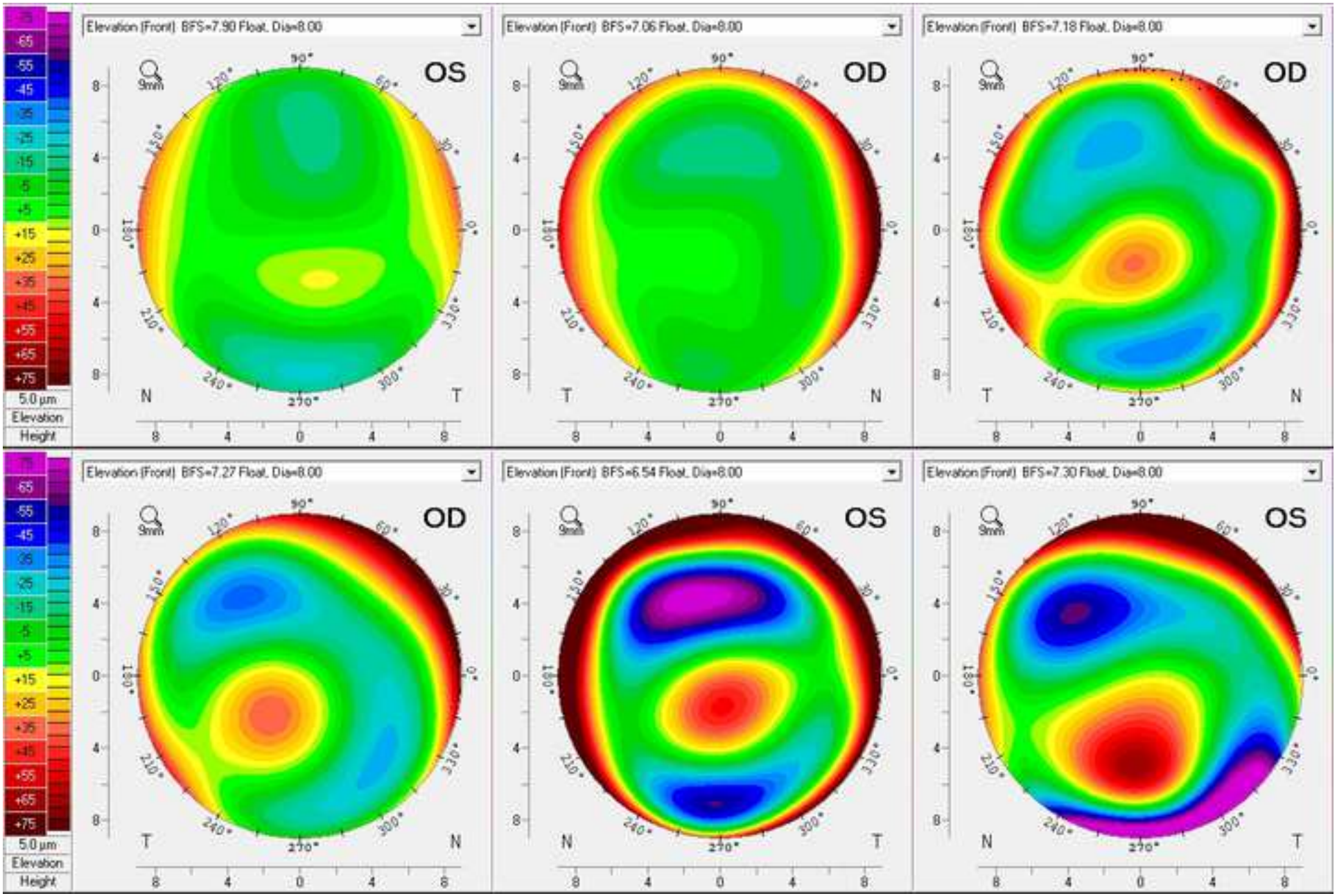

Figure 1D

Click here to access/download;Figure;Figure1D.tiff

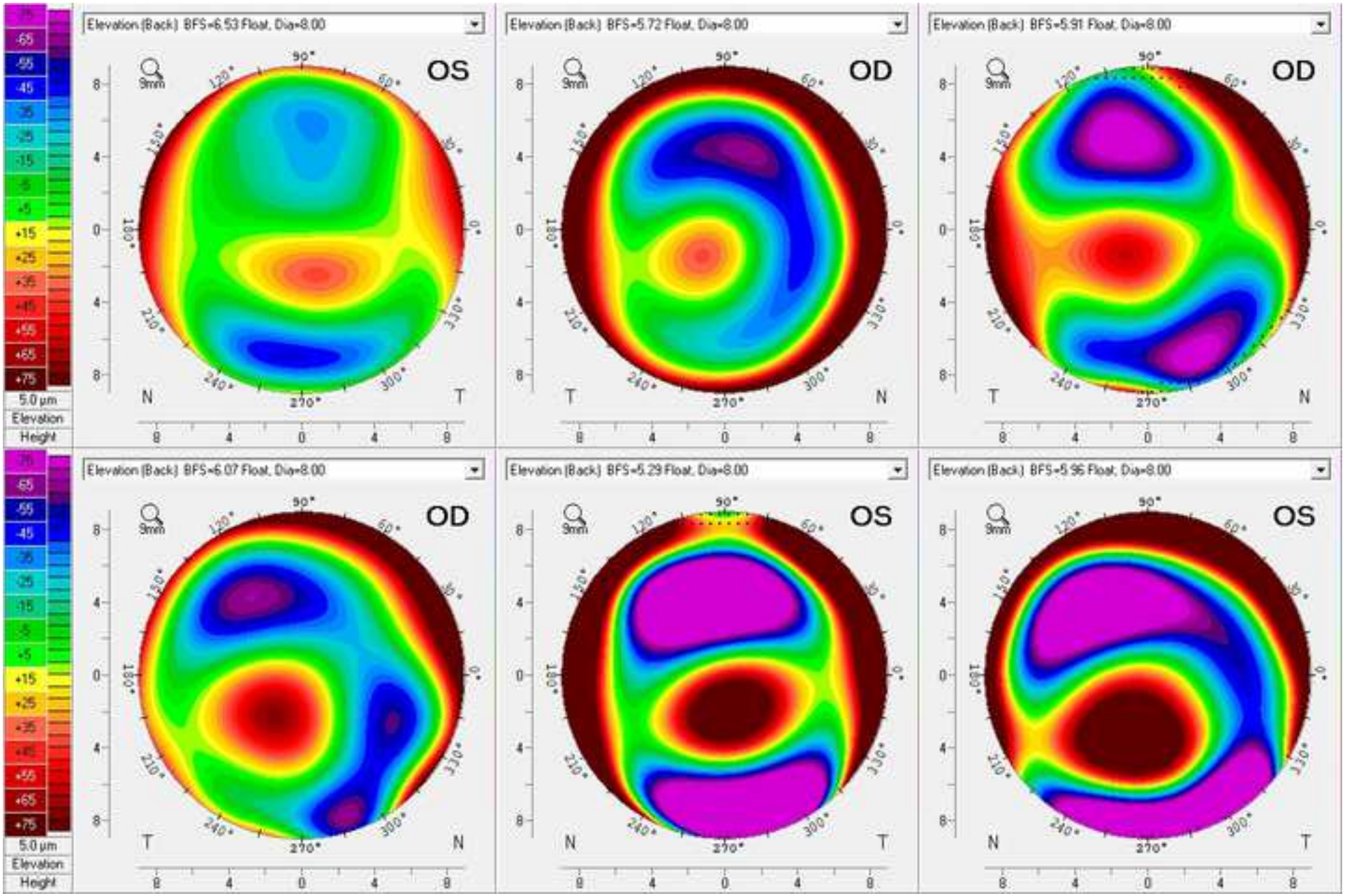

Figure 2A

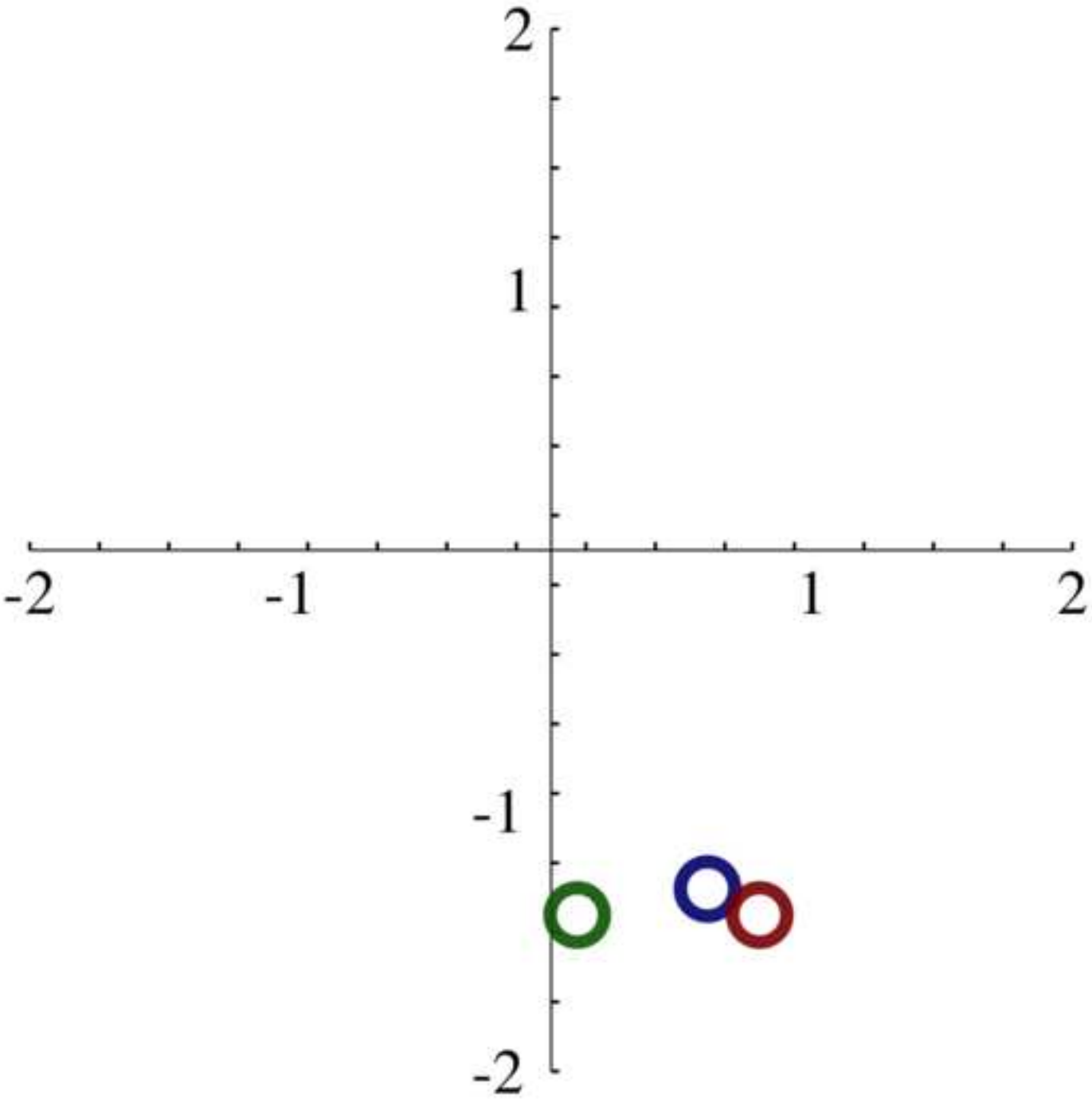

Figure 2B

Click here to access/download;Figure;Figure2B.tiff

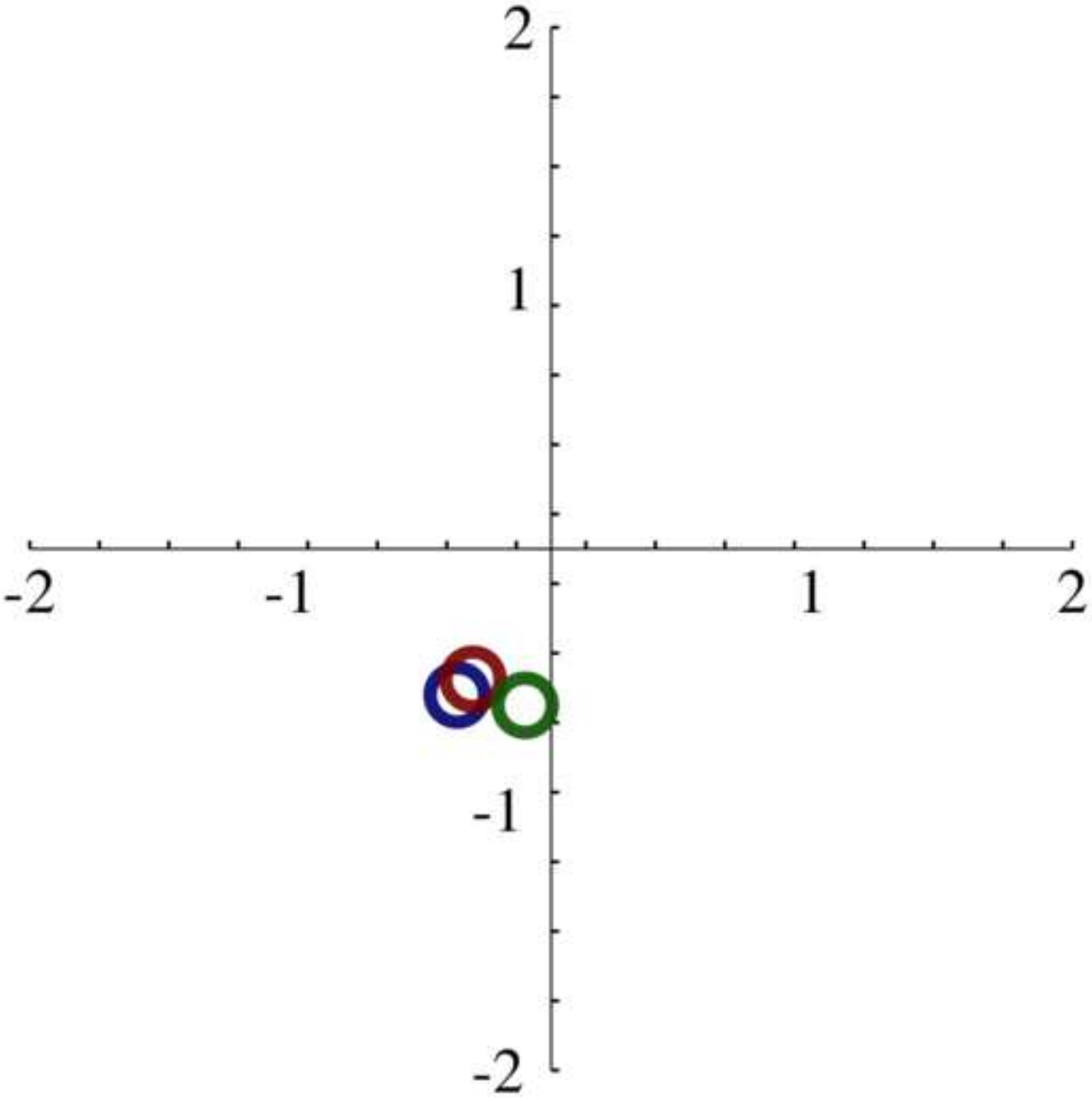

Figure 2C

Click here to access/download;Figure;Figure2C.tiff

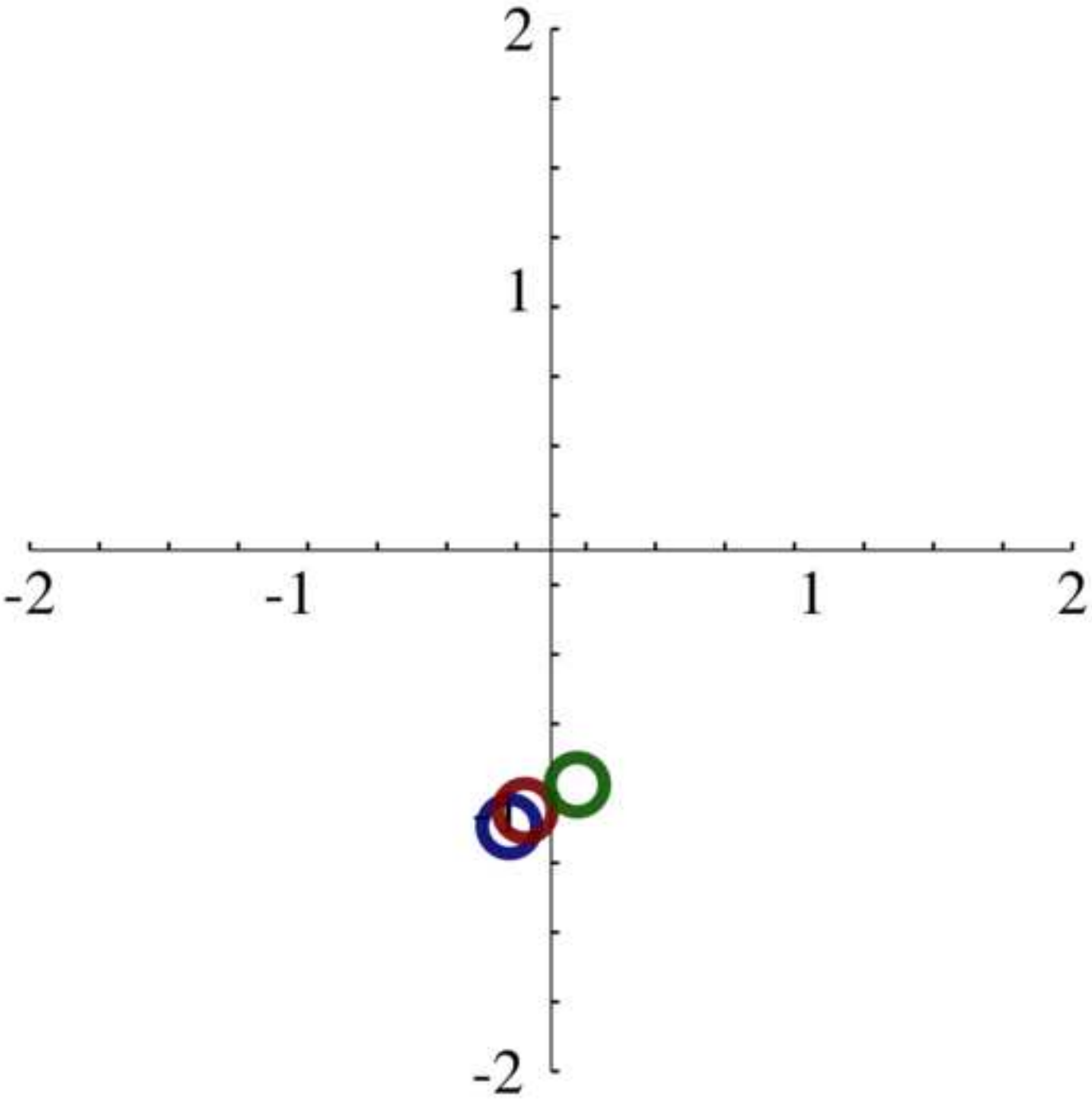

Figure 2D

Click here to access/download;Figure;Figure2D.tiff

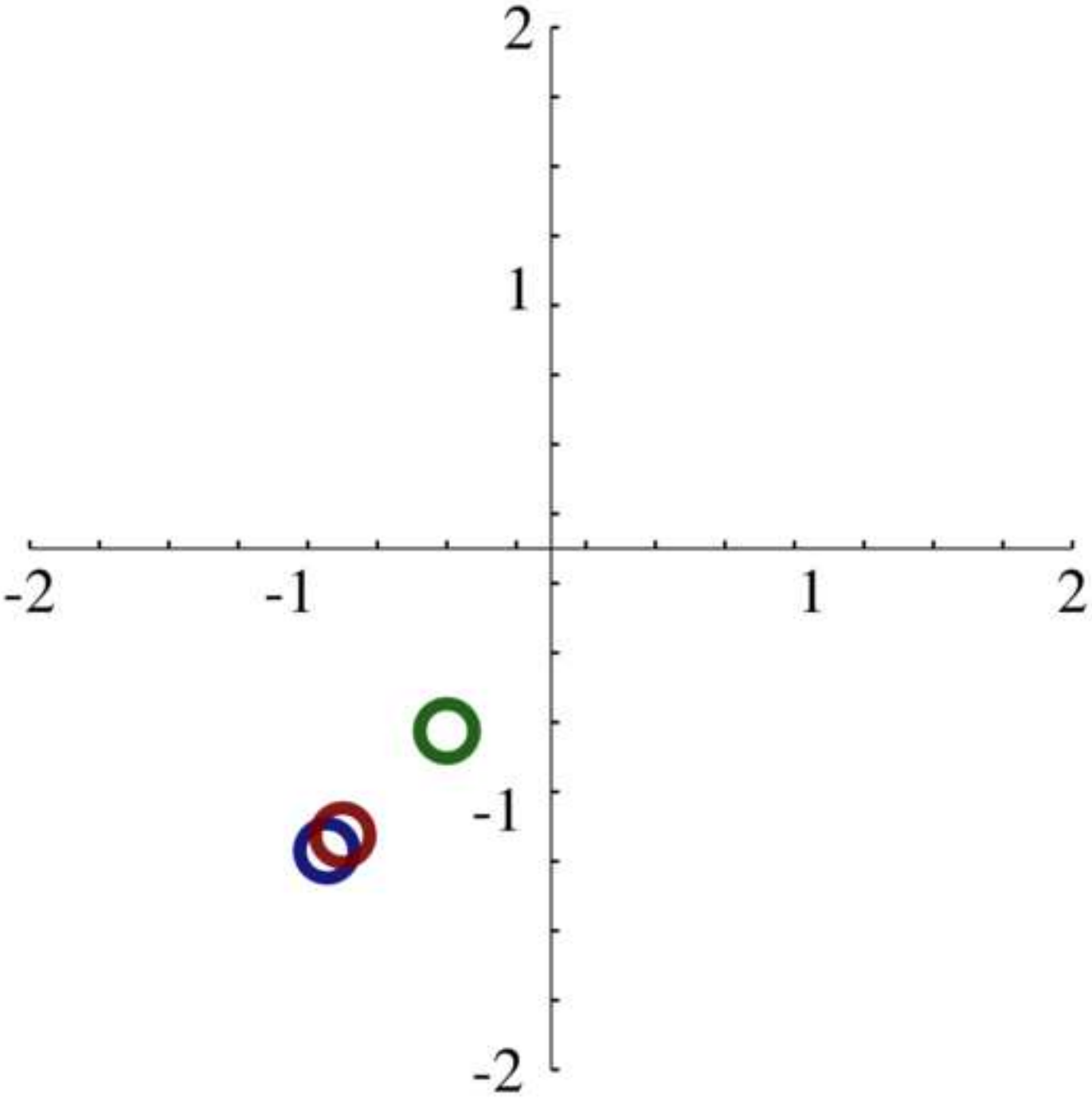

Figure 2E

Click here to access/download;Figure;Figure2E.tiff

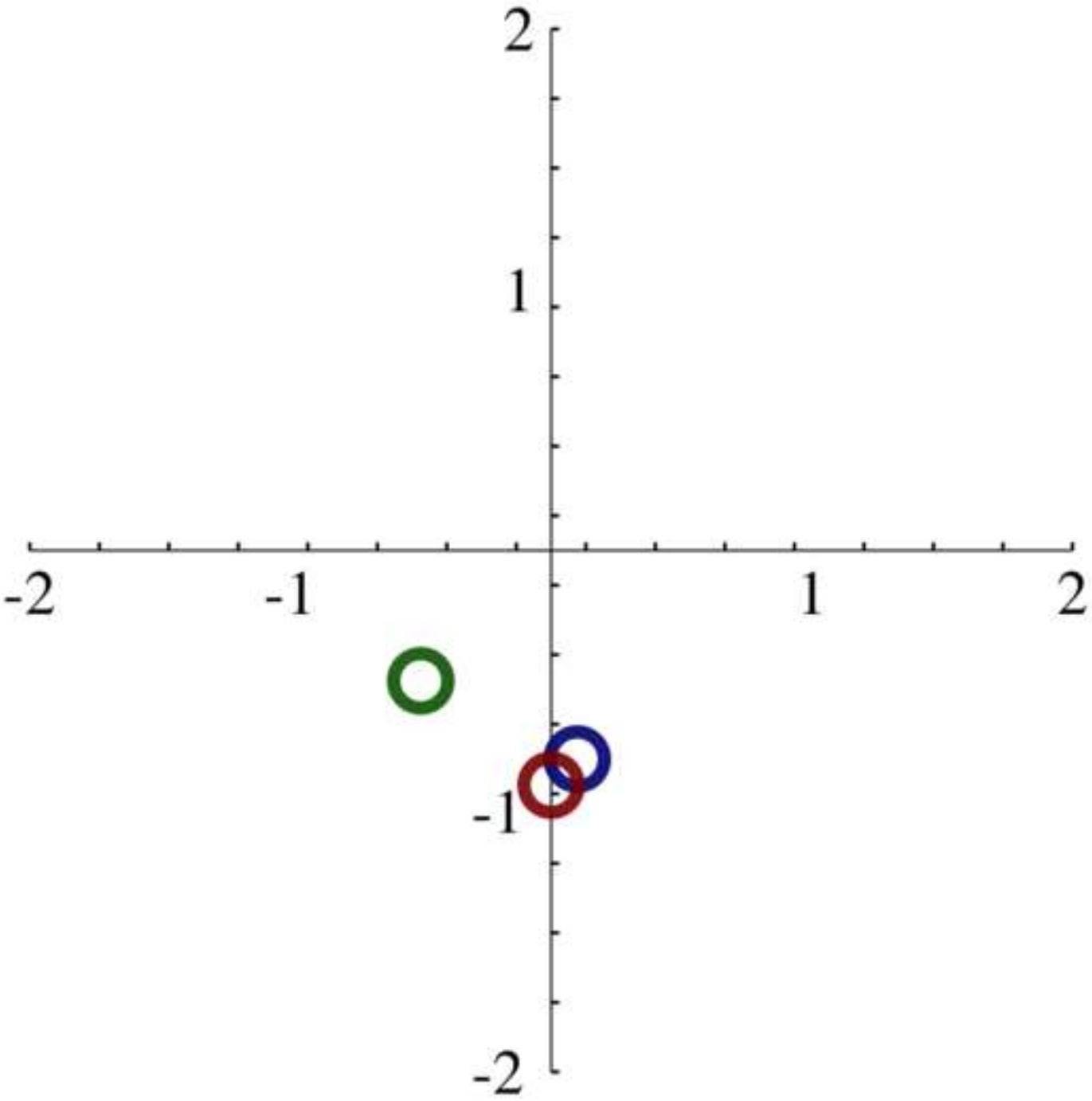

Figure 2F

Click here to access/download;Figure;Figure2F.tiff

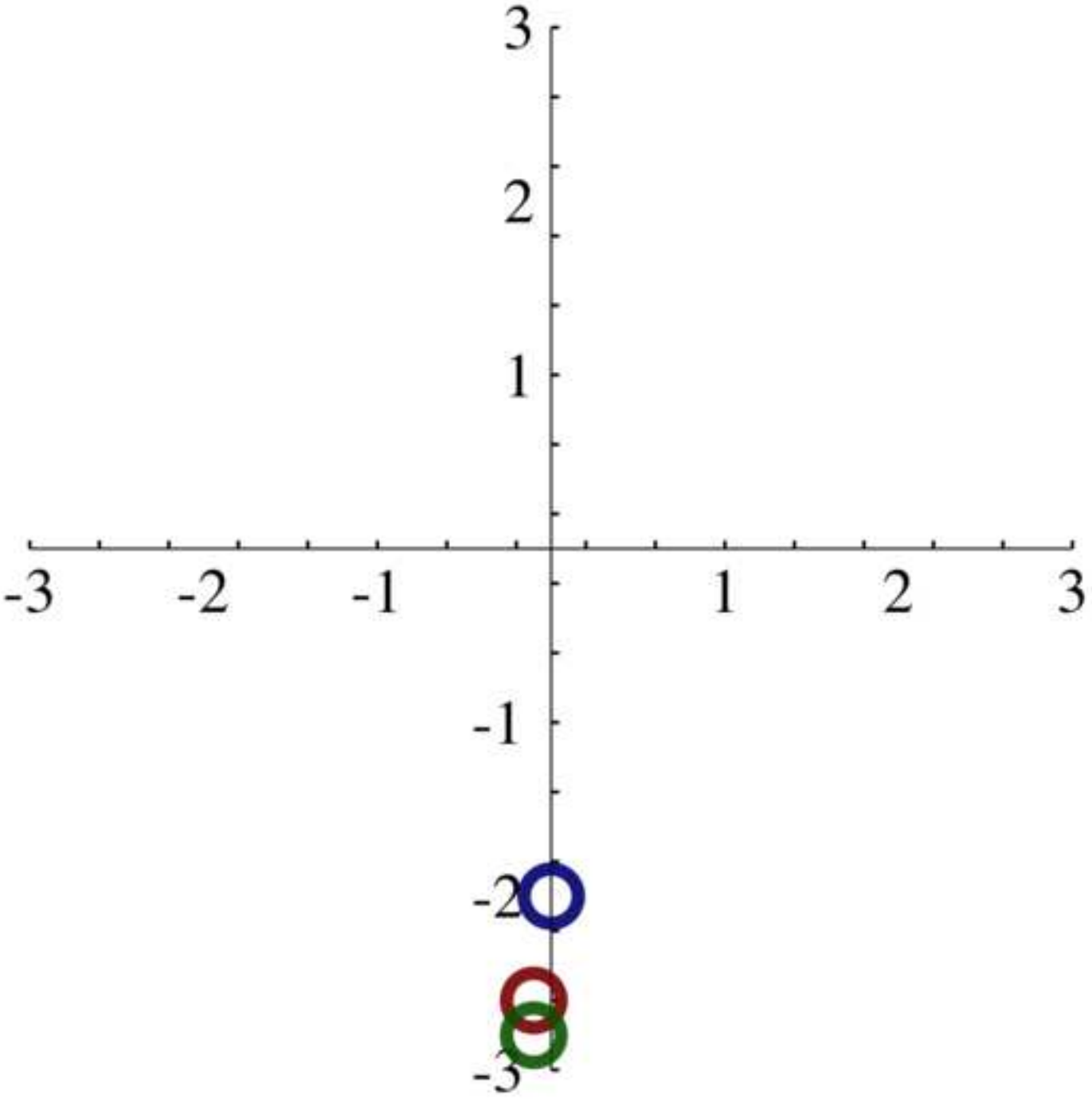

Figure 2G

Click here to access/download;Figure;Figure2G.tiff

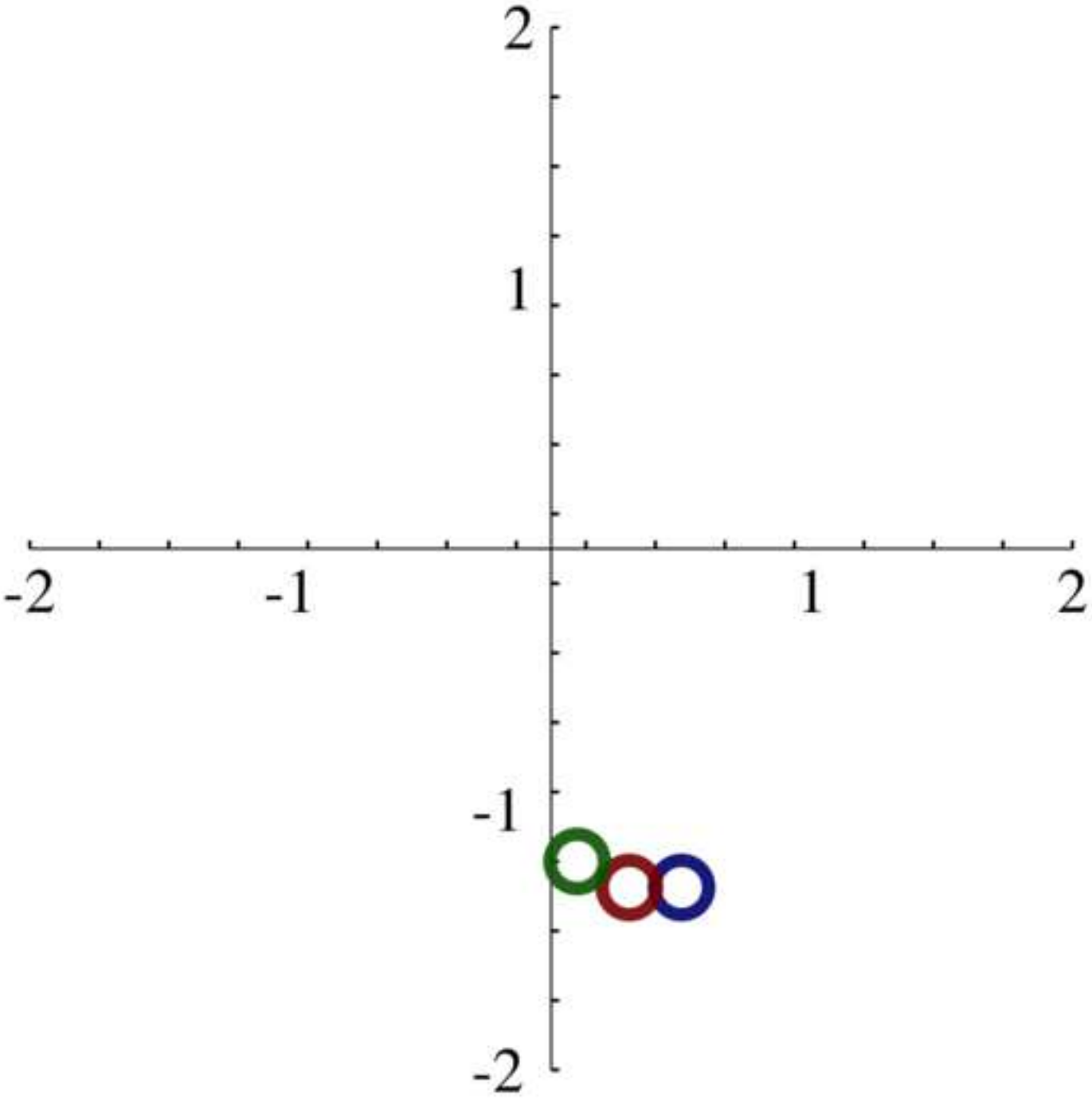

Figure 2H

Click here to access/download;Figure;Figure2H.tiff

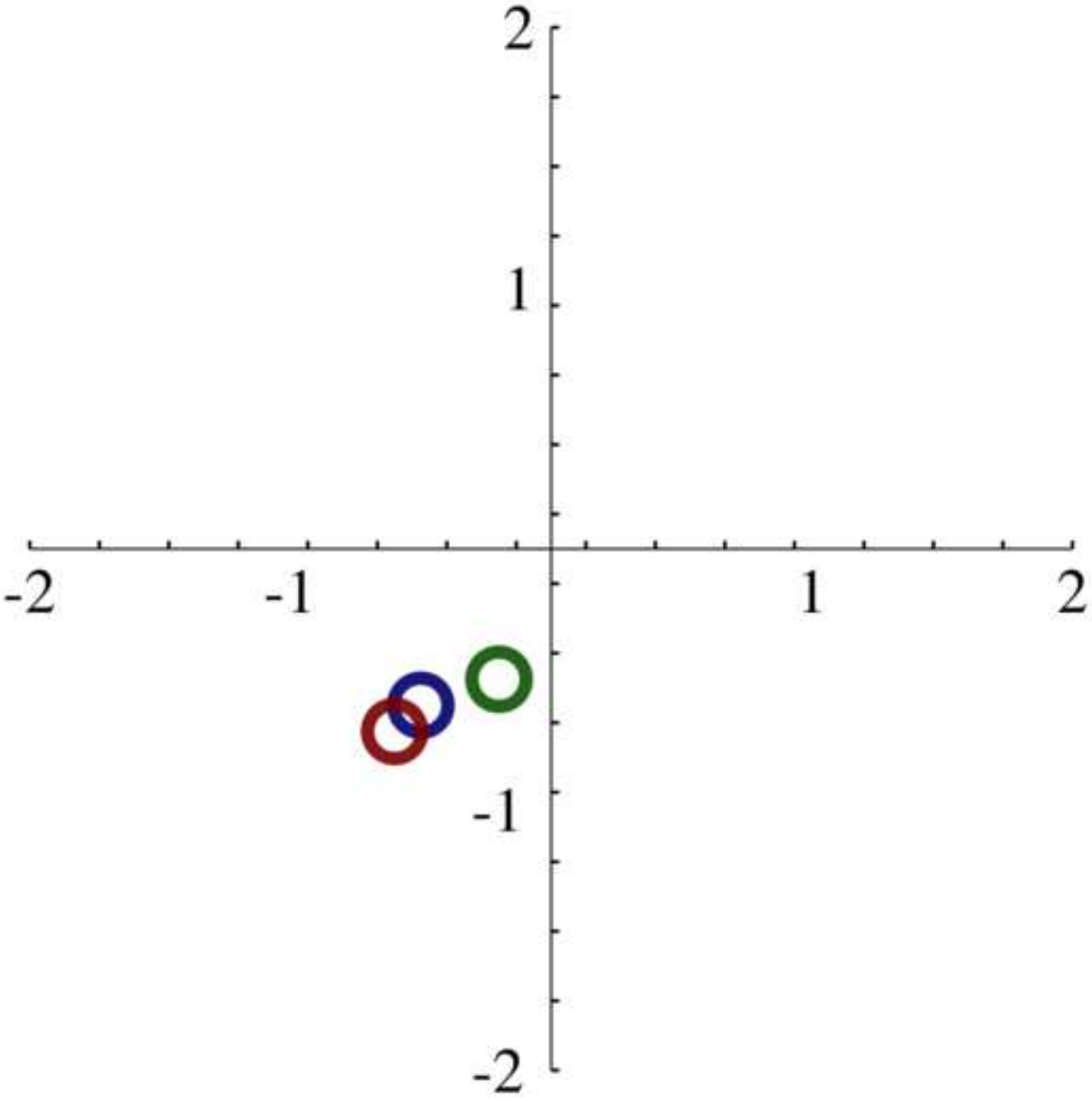

Figure 2I

Click here to access/download;Figure;Figure2I.tiff

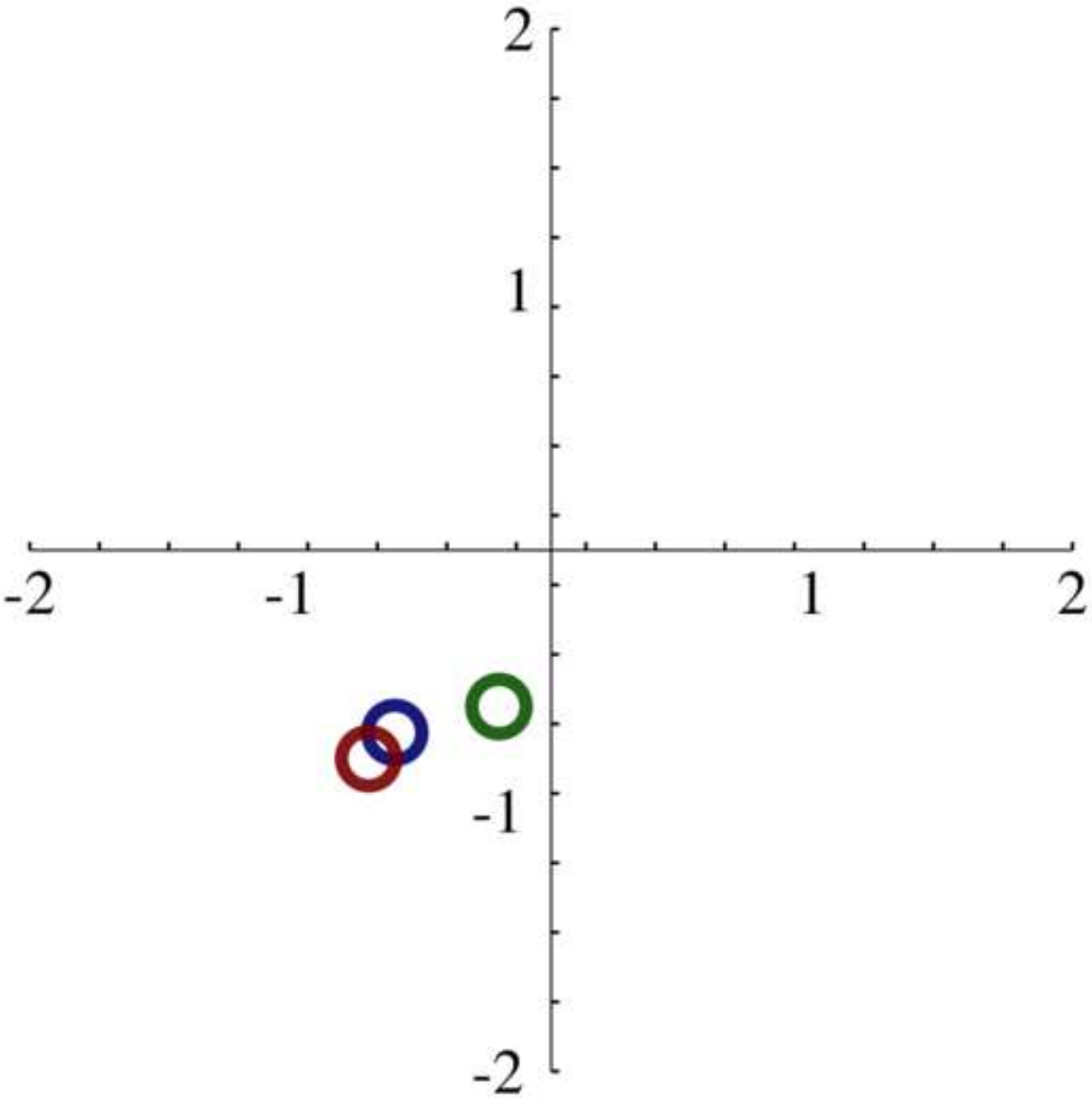

Figure 2J

Click here to access/download;Figure;Figure2J.tiff

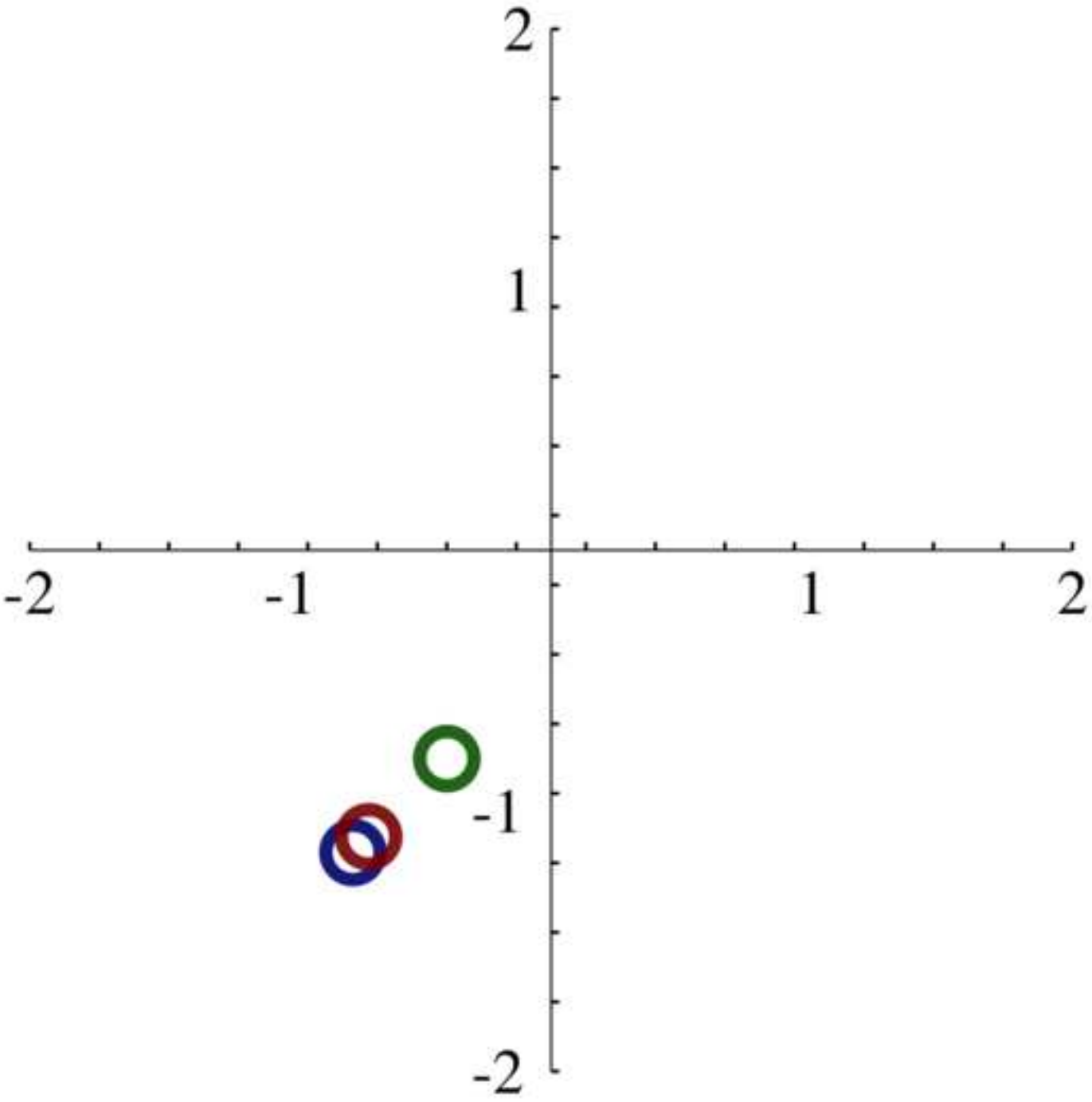

Figure 2K

Click here to access/download;Figure;Figure2K.tiff

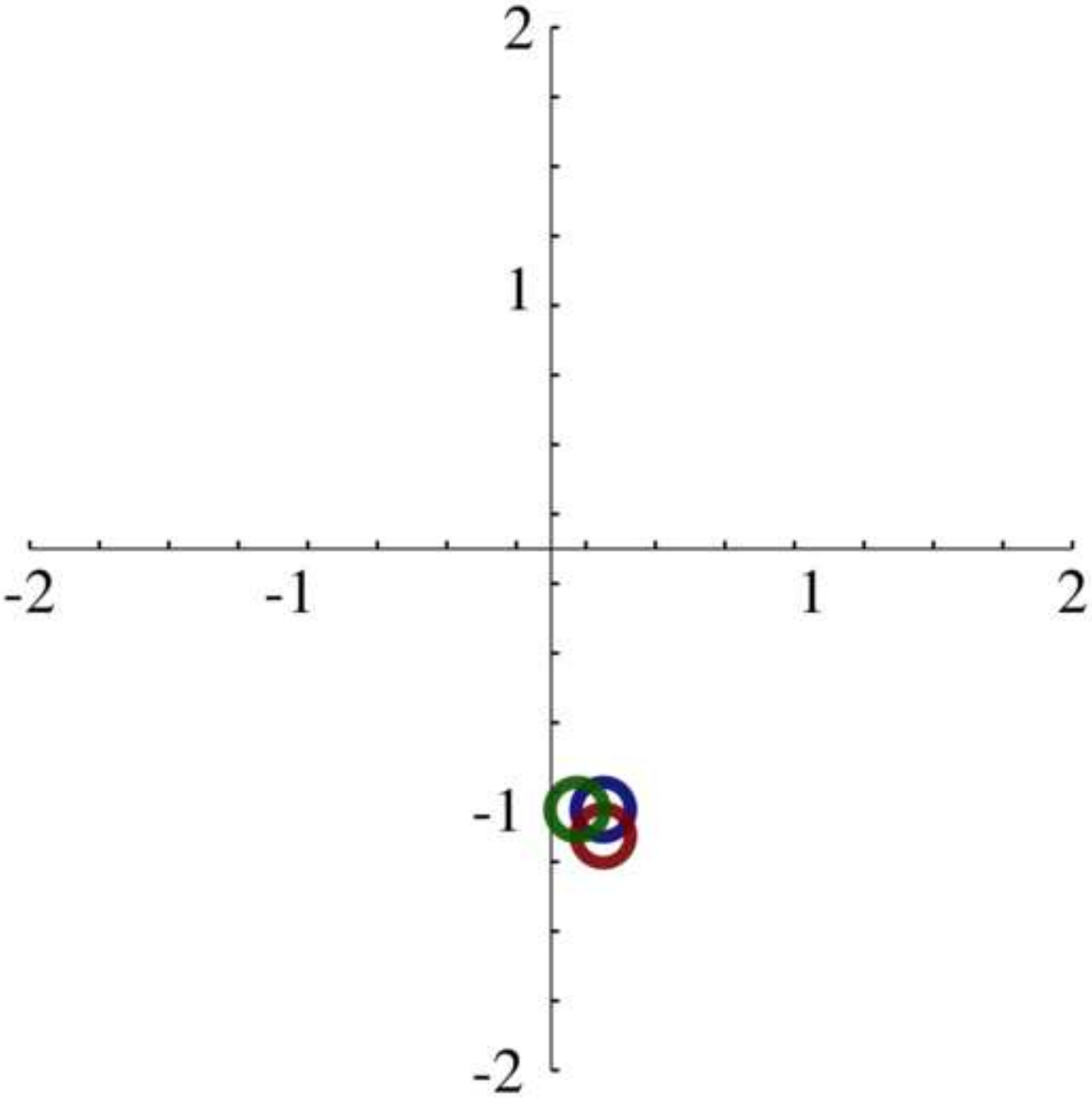

Figure 2L

Click here to access/download;Figure;Figure2L.tiff

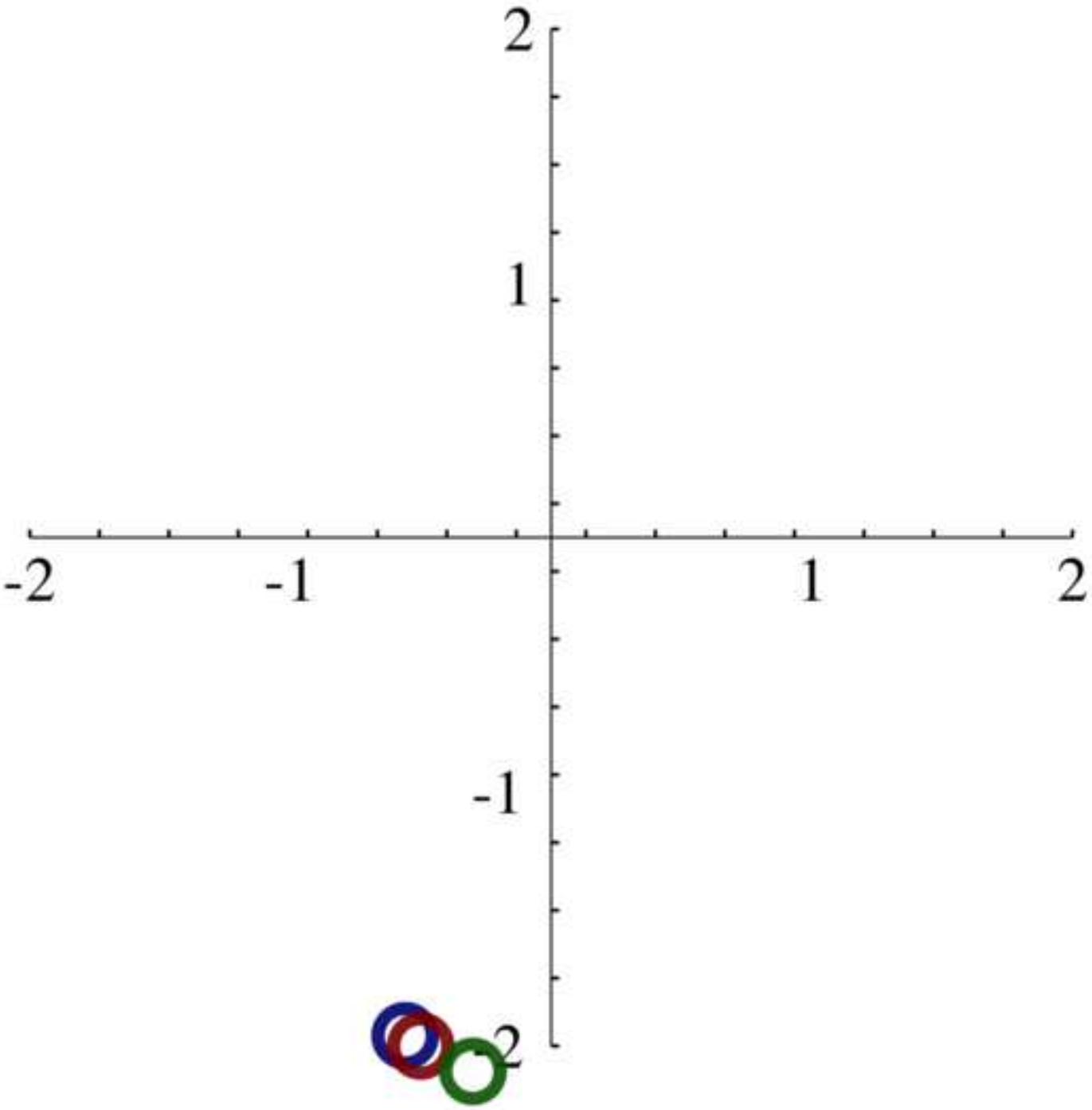

Figure 3A

Click here to access/download;Figure;Figure3A.tif

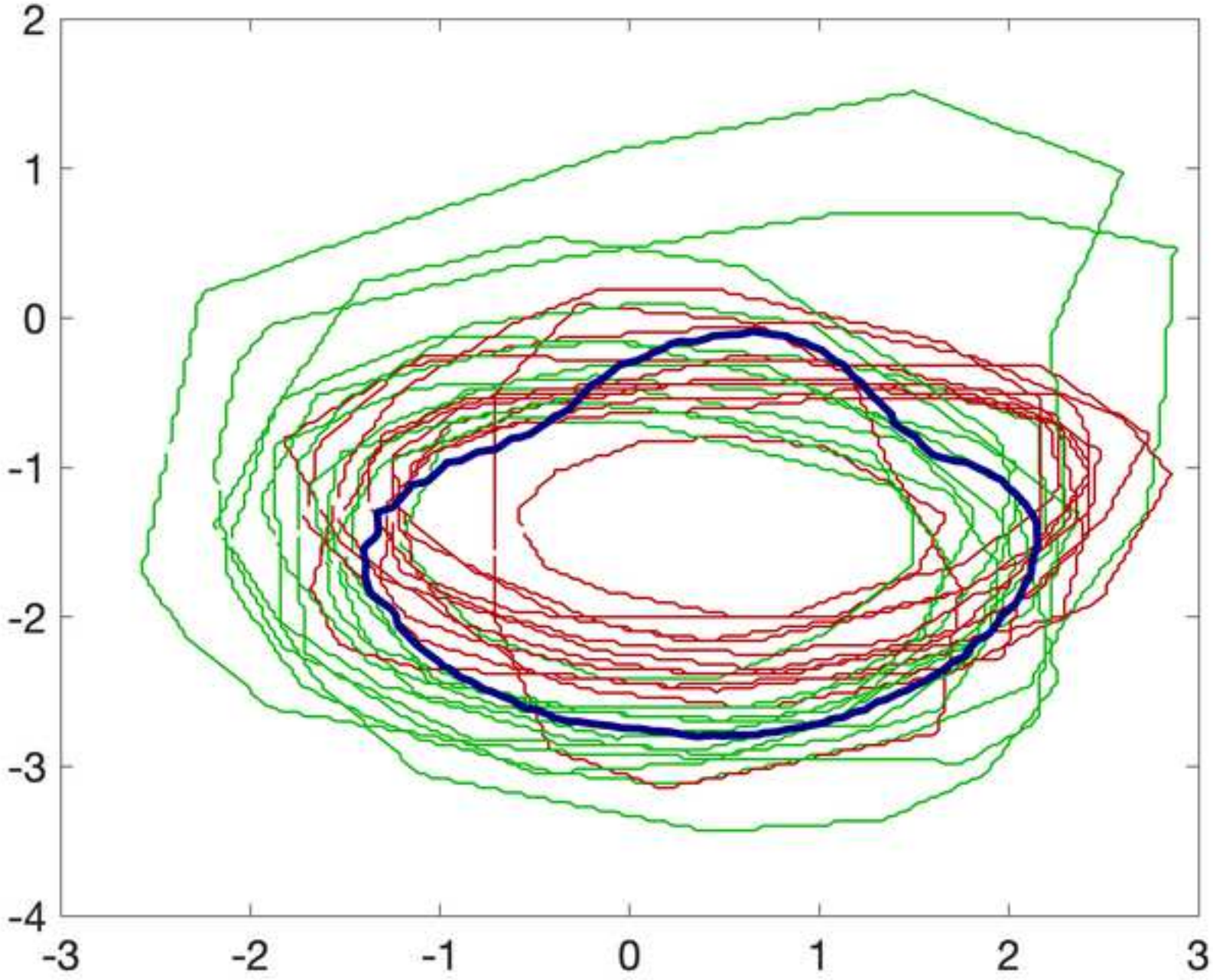

Figure 3B

Click here to access/download;Figure;Figure3B.tif

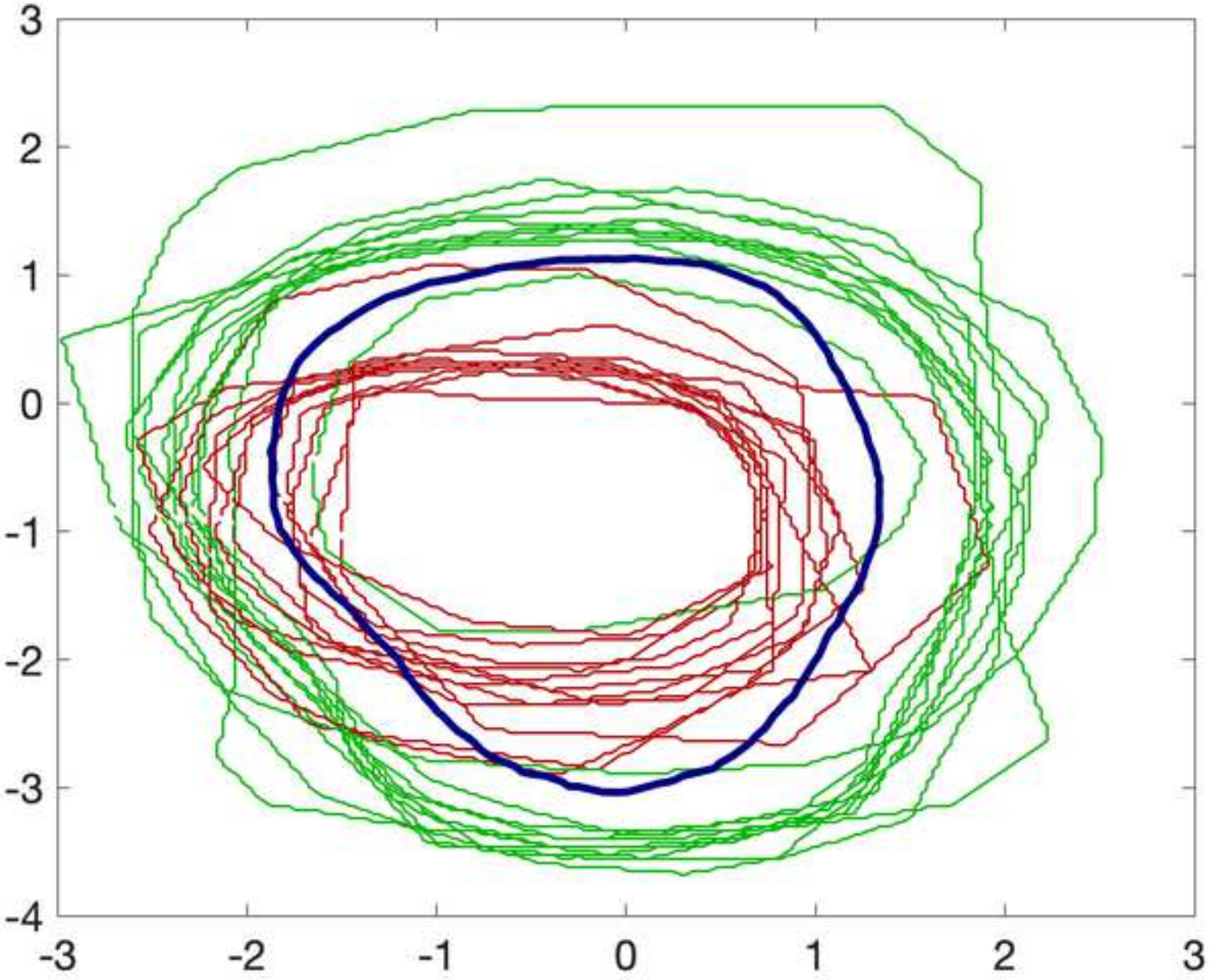

Figure 3C

Click here to access/download;Figure;Figure3C.tif

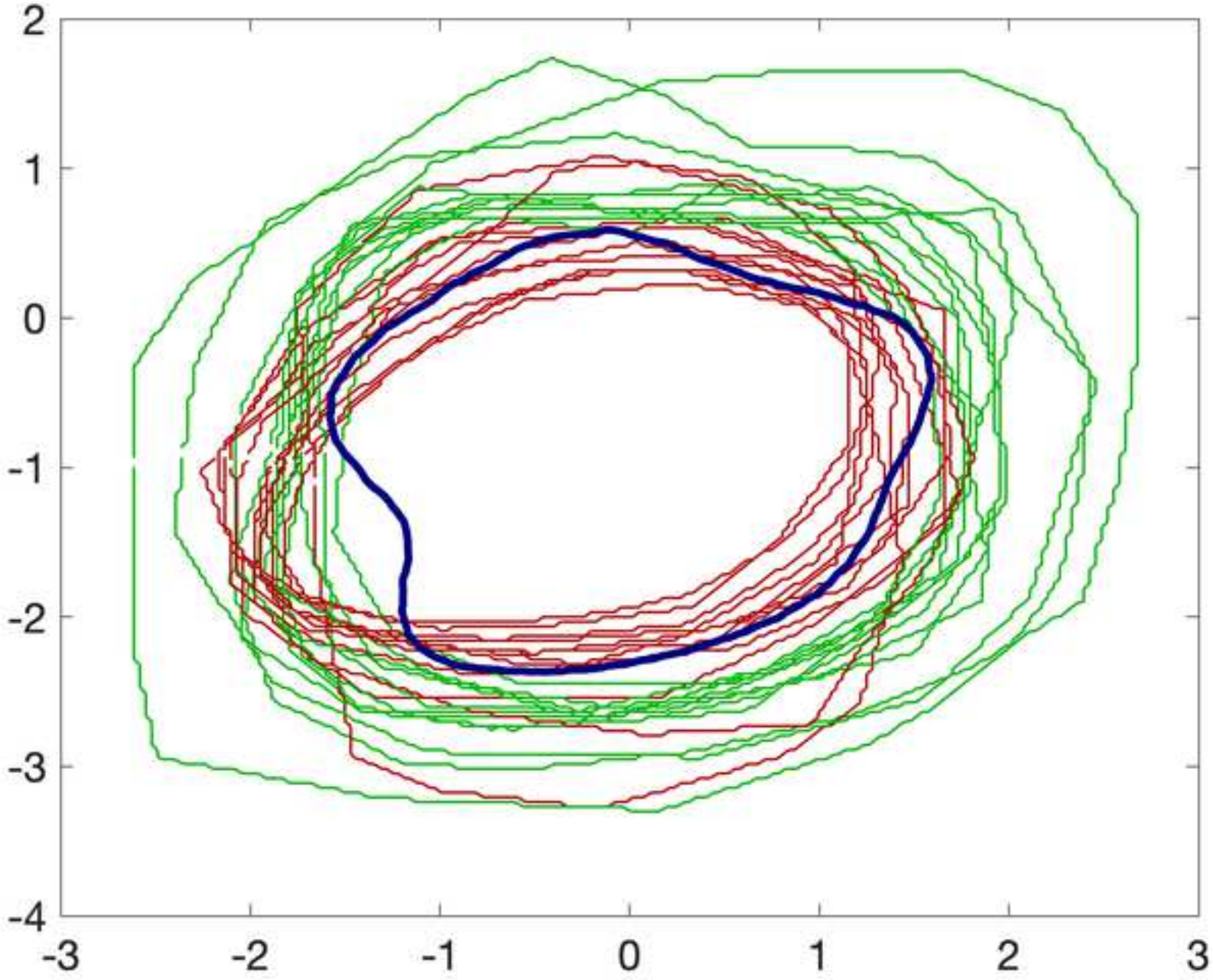

Figure 3D

Click here to access/download;Figure;Figure3D.tif

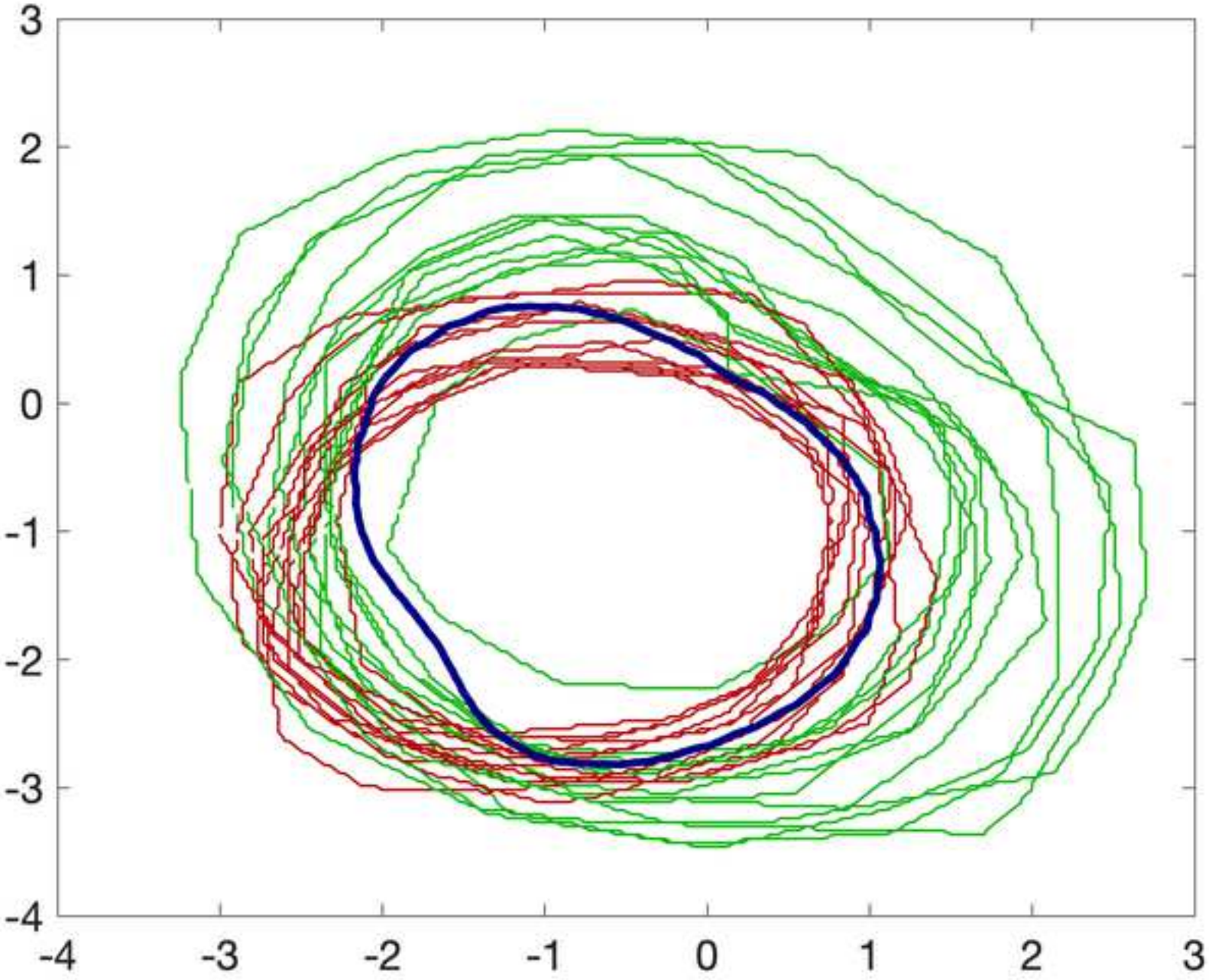

Figure 3E

Click here to access/download;Figure;Figure3E.tif

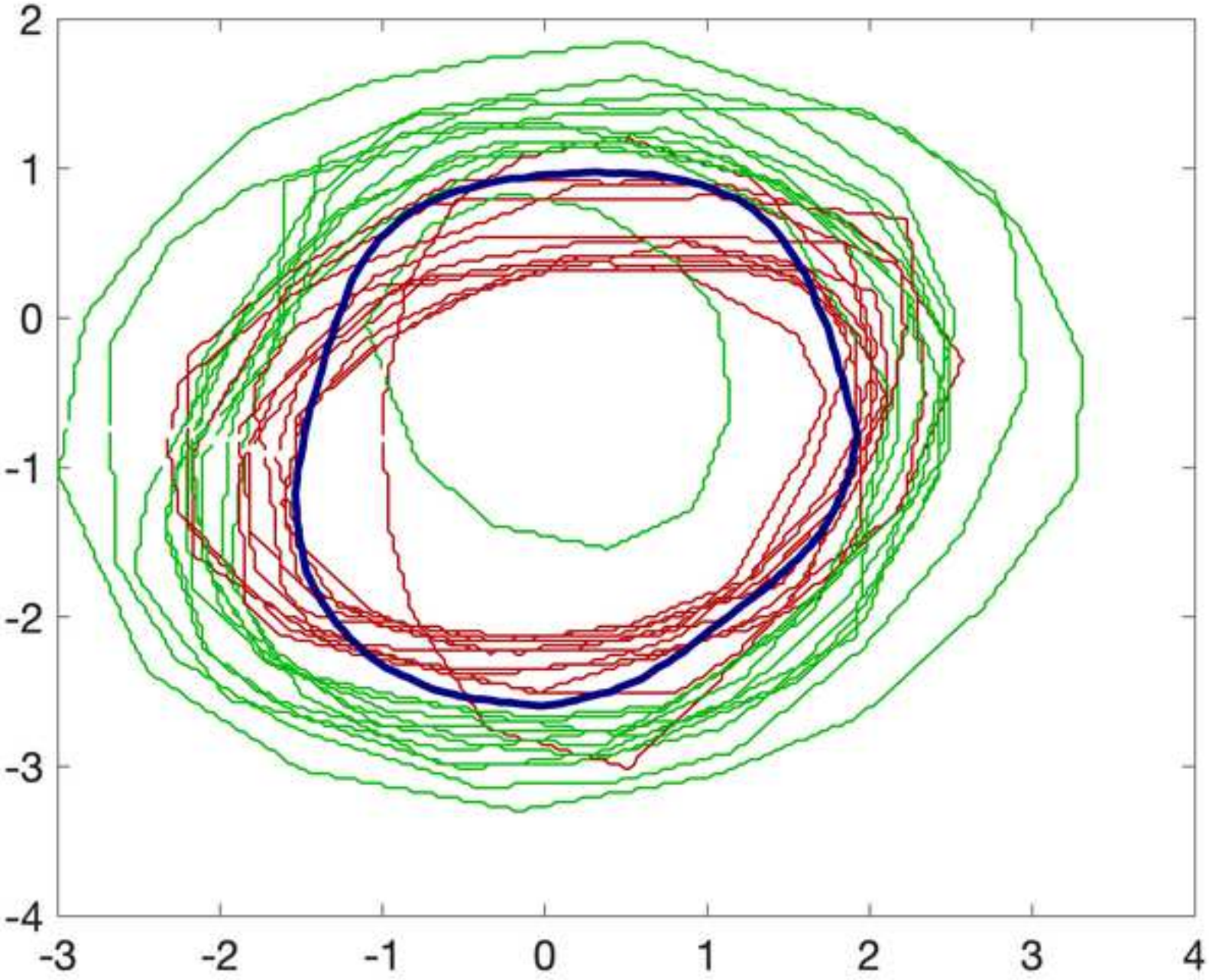

Figure 3F

Click here to access/download;Figure;Figure3F.tif

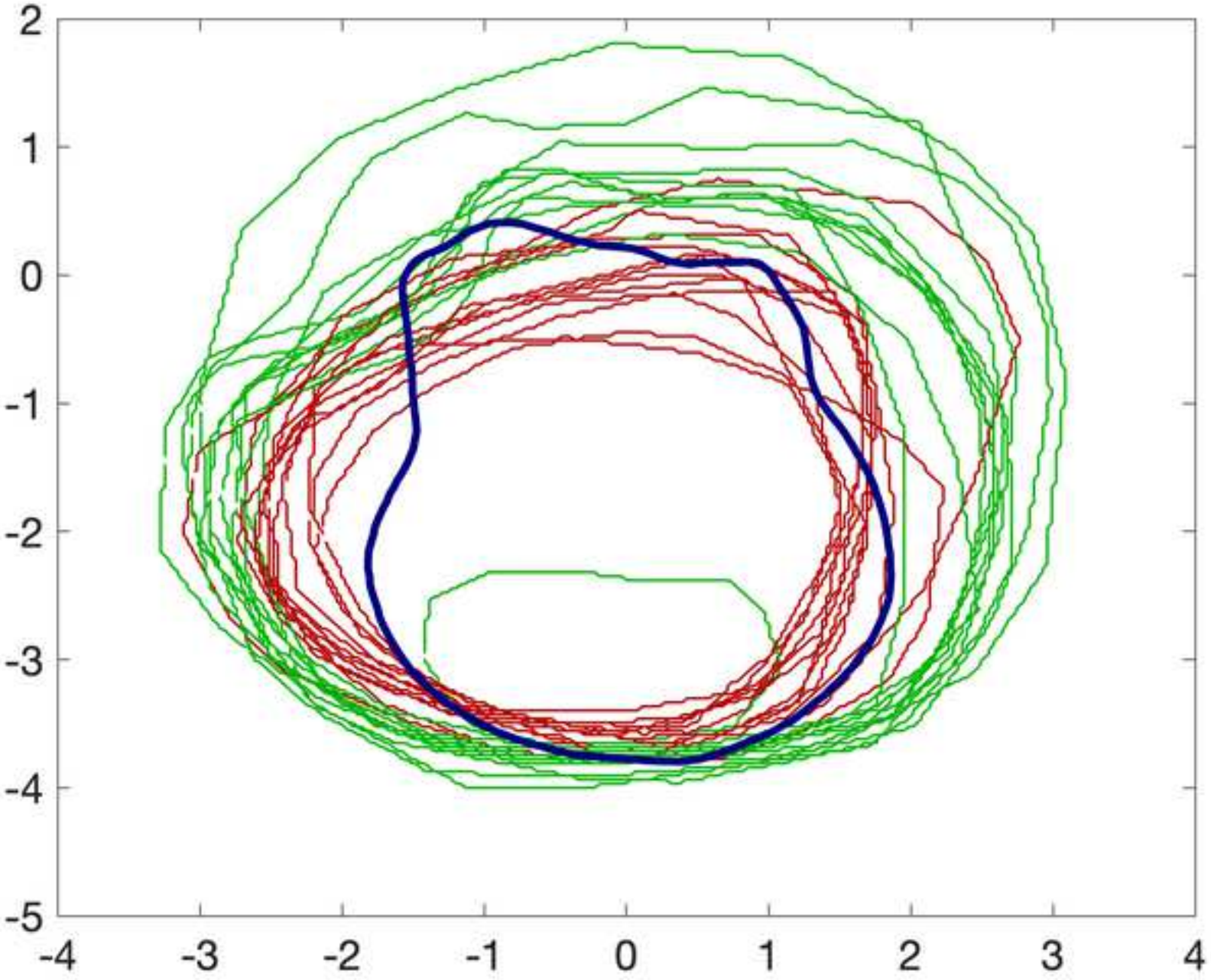

Figure 3G

Click here to access/download;Figure;Figure3G.tif

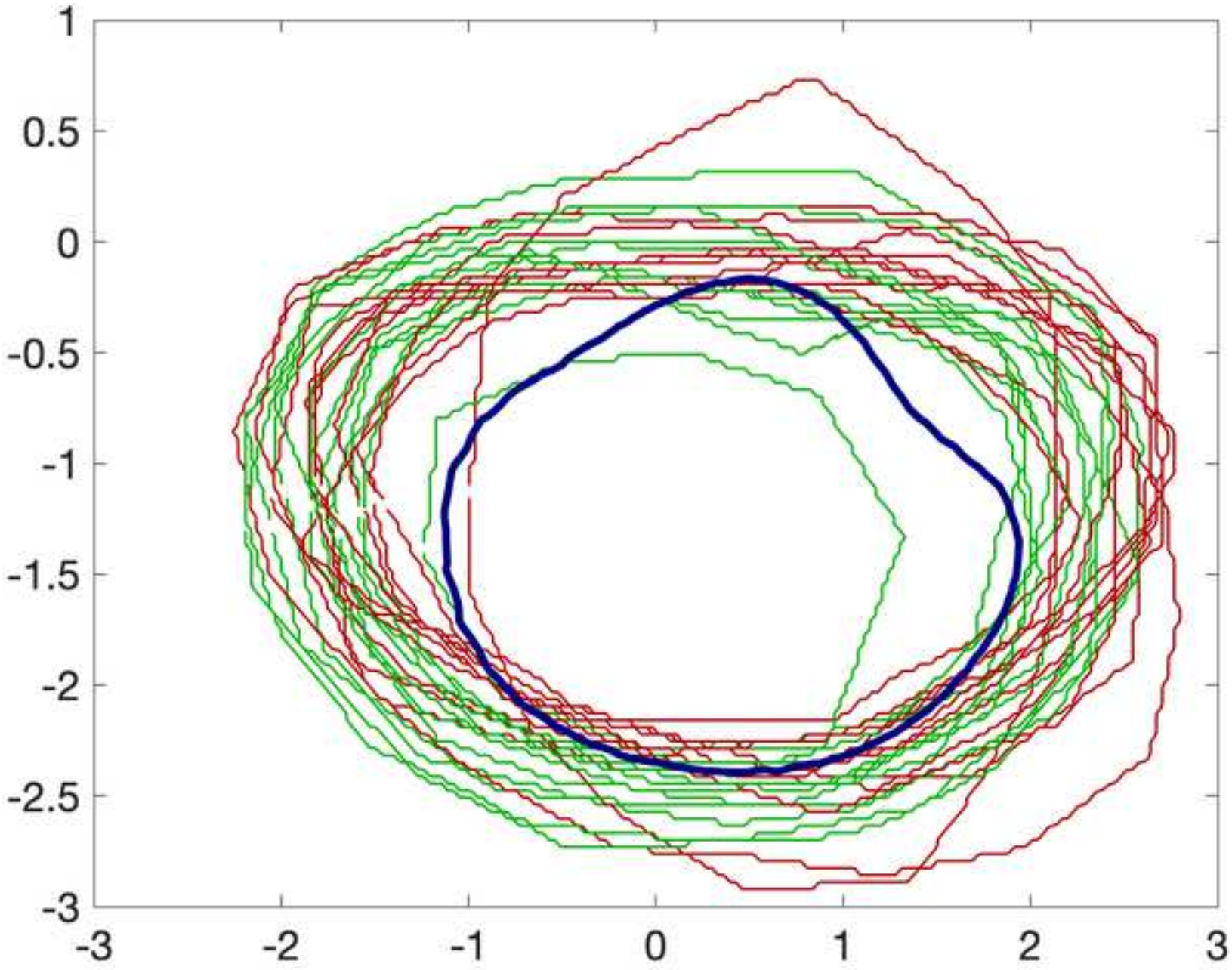

Figure 3H

Click here to access/download;Figure;Figure3H.tif

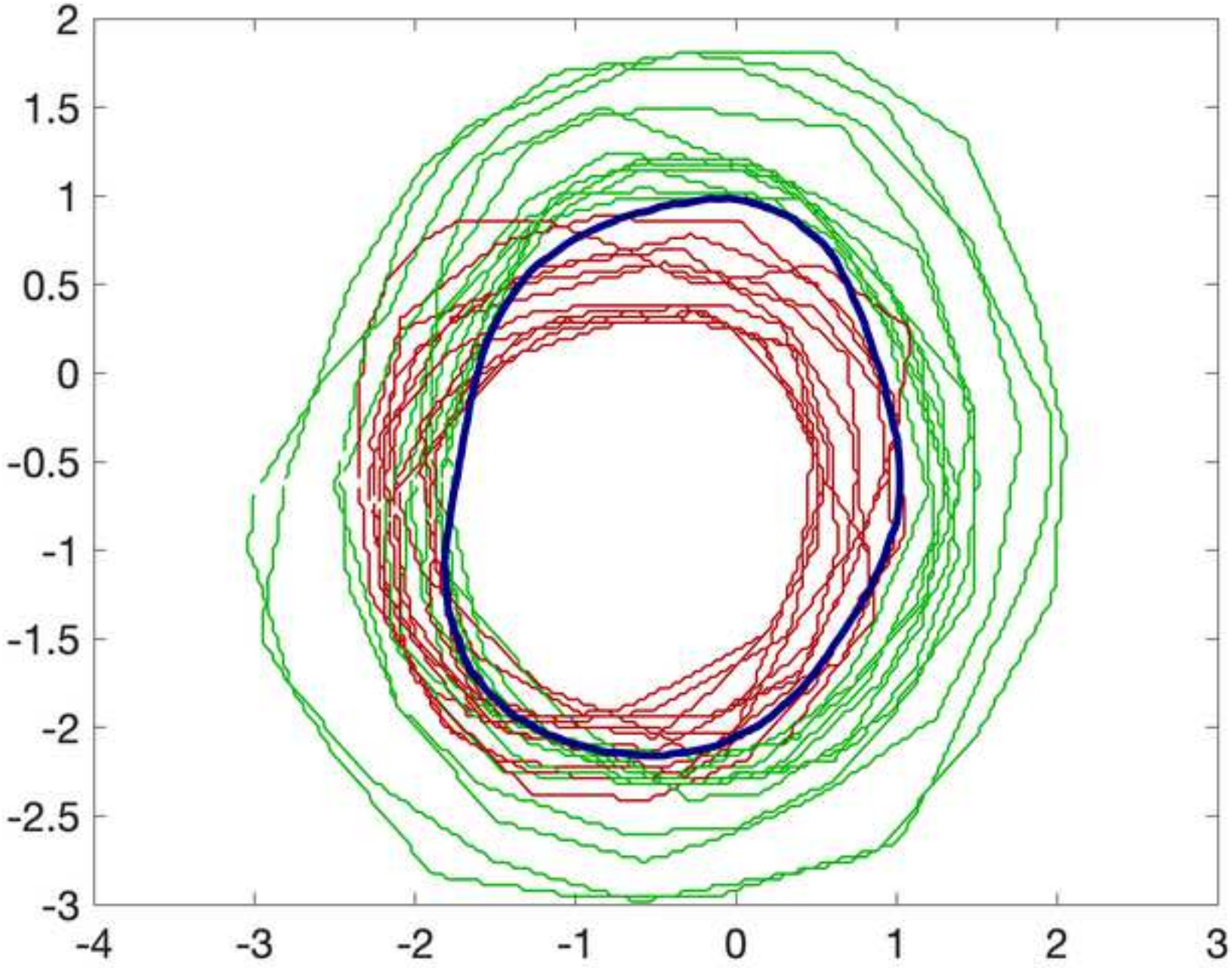

Figure 3I

Click here to access/download;Figure;Figure3I.tif

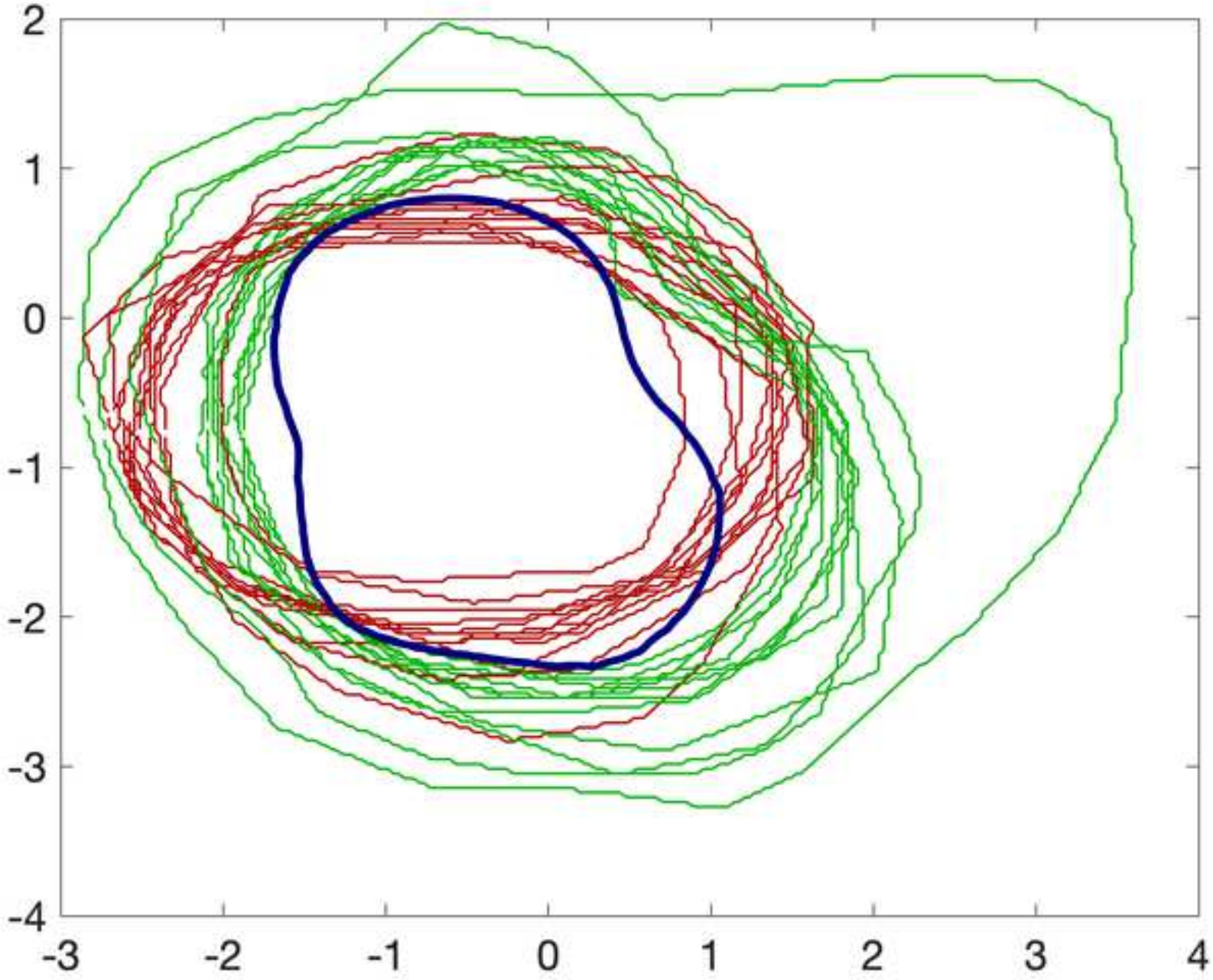

Figure 3J

Click here to access/download;Figure;Figure3J.tif

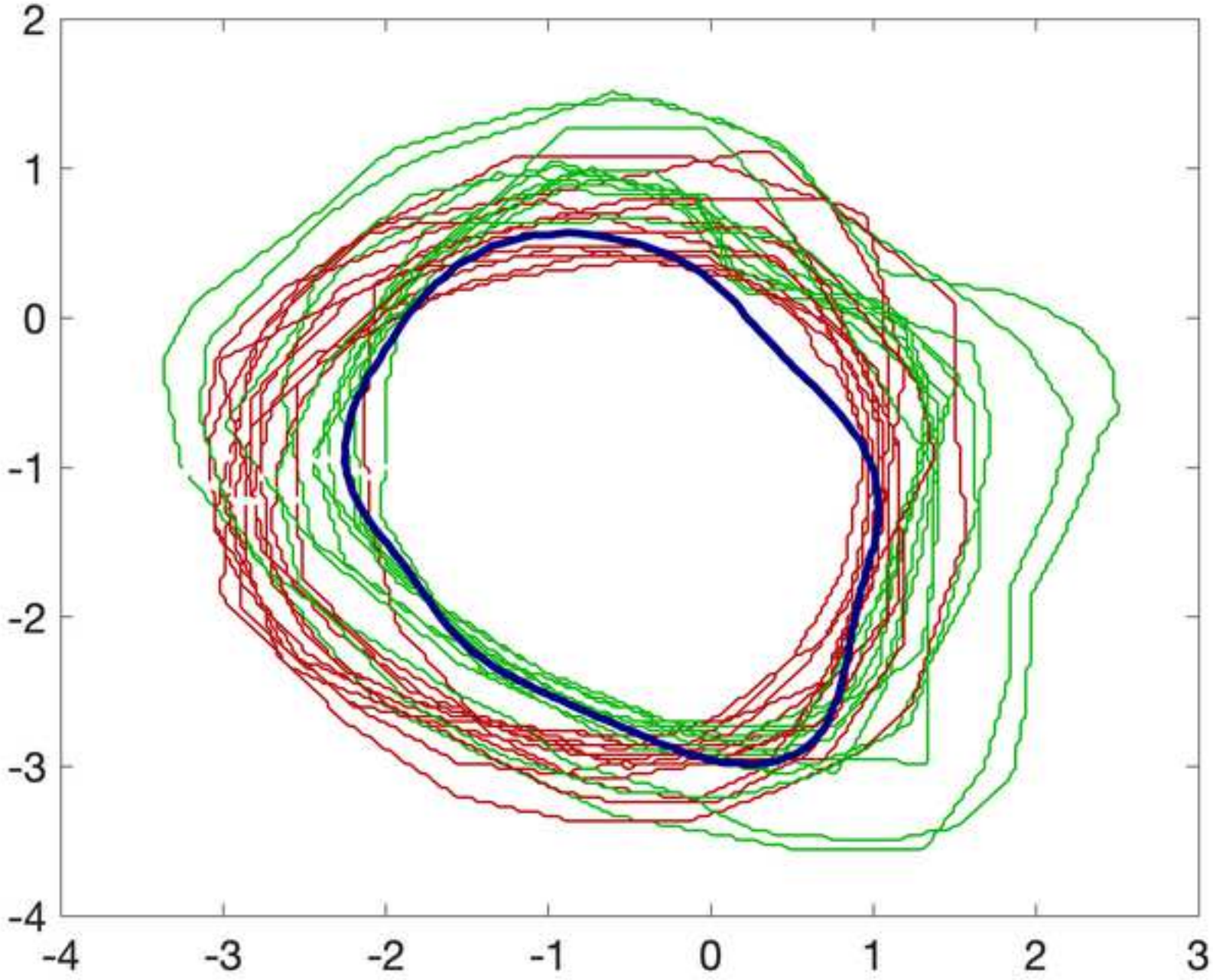

Figure 3K

Click here to access/download;Figure;Figure3K.tif

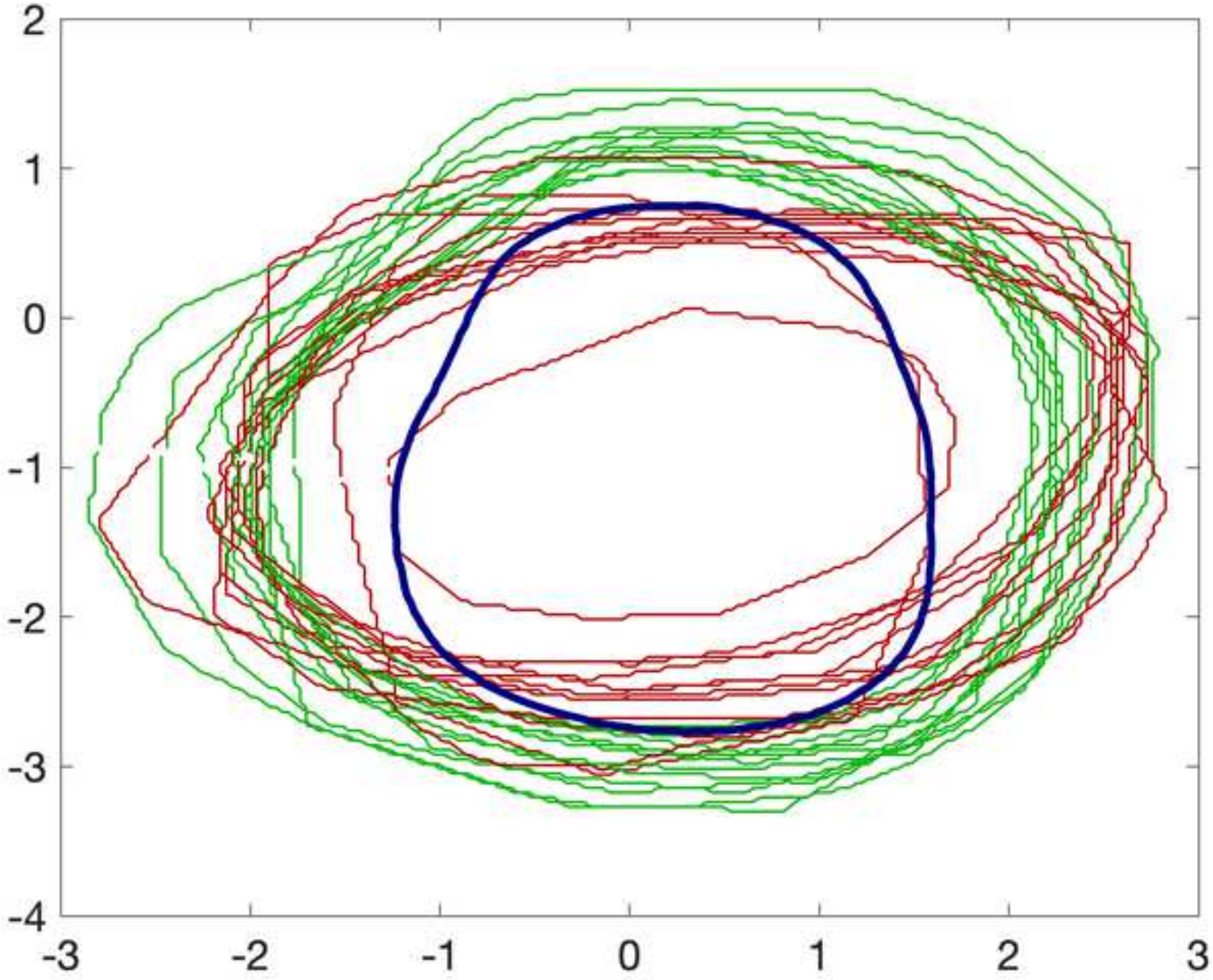

Figure 3L

Click here to access/download;Figure;Figure3L.tif